

Dissipative dynamics in a quantum bistable system: crossover from weak to strong damping

Luca Magazzù,^{1,2,*} Davide Valenti,^{1,†} Bernardo Spagnolo,^{1,2,3,‡} and Milena Grifoni^{4,§}

¹*Dipartimento di Fisica e Chimica, Università di Palermo,
Viale delle Scienze Edificio 18, I-90128 Palermo, Italy*

²*Radiophysics Department, Lobachevsky State University of Nizhni Novgorod, Russia*

³*Istituto Nazionale di Fisica Nucleare, Sezione di Catania, Italy*

⁴*Theoretische Physik, Universität Regensburg, 93040 Regensburg, Germany*

(Dated: August 28, 2022)

The dissipative dynamics of a quantum bistable system coupled to a Ohmic heat bath is investigated beyond the spin-boson approximation. We propose a novel approximation scheme, based on a real-time path integral approach, which enables to capture the system's dynamics over a wide range of temperatures T and coupling strengths γ . Exploiting a separation of time scales between the intra-well and inter-well (tunneling) dynamics, a set of coupled integro-differential equations for the populations in a space localized basis is obtained. A phase-diagram in the (γ, T) space identifying regions of coherent and incoherent dynamics as well as of bath induced localization is provided.

PACS numbers: 03.65.Yz, 05.40.-a, 85.25-j

I. INTRODUCTION

Many quantum systems of interest in disparate areas of physics, ranging from particle physics to condensed matter or chemical physics, are characterized by the presence of two minima of potential energy separated by a potential barrier. In the classical regime, if the barrier crossing is not thermally induced, a non-driven particle settles indefinitely in a potential minimum. In contrast, in the quantum regime, the particle is confined in one potential well until the escape by tunneling occurs, even at zero temperature.

A prominent example is that of a flux quantum in a superconducting circuit, tunneling through the effective potential barrier created by a Josephson junction [1, 2].

Other multi-state bistable systems which received much attention, as candidate for both classical and quantum computing hardware, are molecular nanomagnets [3, and references therein]. The experimental signature of thermally induced tunneling of magnetization in these high spin molecules is the presence of resonant peaks in the transfer rate from a metastable state, as a function of an applied static bias. Moreover, asymmetric bistable systems are used to investigate the relaxation from a quantum metastable state [4–8].

Depending on the potential barrier, which in some case (e.g. in superconducting devices) can be manipulated, the tunneling dynamics takes place on time scales much larger than those associated to the intra-well motion. This allows for the coherent manipulation of the state for quantum simulations or quantum computing

purposes [9–13].

However, real systems are always in contact with dissipative environments and thus subject to relaxation and decoherence, so that it is important to characterize the noise sources and their influence on the dynamics and coherence properties [14, 15].

In general, if the system was prepared, say, in the left well, coherent Rabi oscillations between the two metastable wells occur at very small dissipation strengths and low temperatures. On the other hand, at sufficiently large damping and/or high temperatures the dynamics is known to be incoherent. So far, the coherent to incoherent crossover has been only investigated in the so-called two-level system (TLS) approximation for the Hilbert space of the bistable system: the temperature is taken to be low enough that, to a good approximation, the system's dynamics can be restricted to the space spanned by the lowest doublet $\{|g\rangle, |e\rangle\}$ of eigenstates of the system's bare Hamiltonian (cf. Fig. 1). A vast literature exists [14–16] which investigates the coherent to incoherent crossover for various dissipation mechanisms in great detail.

For temperatures of the order of the separation between the lowest and the next lying energy levels, the TLS approximation breaks down and the multi-level nature of the bistable potential cannot be neglected. Despite its relevance for applications, the dissipative bistable dynamics in this temperature regime is so far poorly understood [4, 5, 17–20].

For very small damping strengths, a perturbative Bloch-Redfield approach capturing coherent intra-well and inter-well oscillations is appropriate [19, 20]. In the opposite regime of moderate to large damping and temperatures the dynamics is fully incoherent and is well described in terms of rate equations for the populations of states localized in the wells, with rates obtained within a non-perturbative path integral approach [4]. However, the crossover regime, characterized by moderate damping

* luca.magazzu@unipa.it

† davide.valenti@unipa.it

‡ bernardo.spagnolo@unipa.it

§ milena.grifoni@physik.uni-regensburg.de

and temperatures, presents an unsolved challenge. The major difficulty lies in the fact that, as the tunneling dynamics occurs on a time scale much larger than that of the intra-well dynamics, a hybrid situation can occur where quantum coherence is present at the level of intra-well motion, but is lost at longer times where tunneling processes are relevant.

In this work we develop a novel, non-perturbative in the coupling, approximation scheme which enables to investigate the transient and long time bistable dynamics in the crossover dissipation regime. Similarly to [4, 5], it is based on a real-time path integral approach for the reduced density matrix (RDM) of a quantum particle linearly coupled to a bosonic reservoir. By tracing out the reservoir degrees of freedom, a formally exact expression for the elements of the RDM is obtained, in which the environmental effects are encapsulated in the so-called Feynman-Vernon (FV) influence functional [21]. The latter introduces nonlocal in time correlations between paths, what requires suitable approximation schemes. To take into account the different time scales of the intra- and inter-well dynamics, we include long and short time correlations in the vibrational relaxation (VR) dynamics, while only short time correlations turn out to be relevant for the tunneling process. At low temperature and weak damping, the resulting dynamics exhibits coherent oscillations at short times and incoherent tunneling behavior at longer times. By increasing the temperature and/or coupling strength, a crossover to a fully incoherent regime is observed, in accordance with the predictions in Ref. [4, 5]. Further, localization is predicted at large enough damping [22]. A phase diagram in the coupling strength-temperature plane, displaying the various dynamical regimes, with the corresponding approaches or approximation schemes, gives a comprehensive account for the problem of the dissipative quantum dynamics beyond the TLS approximation.

II. THE MODEL

The system we study is a particle of mass M and coordinates \hat{q} and \hat{p} , subject to a quartic potential $V(q)$. The system interacts linearly with a so-called bosonic heat bath [23], a reservoir of N independent quantum harmonic oscillators, of masses m_j and coordinates \hat{x}_j and \hat{p}_j , initially at thermal equilibrium.

A. Hamiltonian

The full Hamiltonian of the model is

$$\hat{H} = \hat{H}_S + \hat{H}_B + \hat{H}_{SB}, \quad (1)$$

where the bare system Hamiltonian is $\hat{H}_S = \hat{p}^2/2M + V(\hat{q})$. The potential is described by

$$V(\hat{q}) = \frac{M^2\omega_0^4}{64\Delta U}\hat{q}^4 - \frac{M\omega_0^2}{4}\hat{q}^2 - \epsilon\hat{q}, \quad (2)$$

where ϵ is the asymmetry factor and ΔU the barrier height. The terms \hat{H}_B and \hat{H}_{SB} in Eq. (1) describe, according to the Caldeira-Leggett model [23], the free bath energy and the particle-bath interaction energy respectively. In formulae

$$\hat{H}_B + \hat{H}_{SB} = \frac{1}{2} \sum_{j=1}^N \left[\frac{\hat{p}_j^2}{m_j} + m_j\omega_j^2 \left(\hat{x}_j - \frac{c_j}{m_j\omega_j^2} \hat{q} \right)^2 \right].$$

The interaction term features the bilinear coupling $c_j\hat{x}_j\hat{q}$ and a renormalization term $\propto \hat{q}^2$. The latter compensates for the contribution of the oscillators in the effective potential felt by the particle, thus giving a purely dissipative bath.

The bath spectral density function is defined by

$$J(\omega) = \frac{\pi}{2} \sum_{j=1}^N \frac{c_j^2}{m_j\omega_j} \delta(\omega - \omega_j). \quad (3)$$

In the continuum limit $N \rightarrow \infty$, i.e. in the presence of a large, broadband bath, $J(\omega)$ is phenomenologically modeled as a power law in ω , with a high frequency cut-off [14].

In the Heisenberg picture, the equation of motion for \hat{q} is the quantum Langevin equation for the particle subject to the force exerted by the bath, which in the limit $\hbar \rightarrow 0$ reproduces the classical colored noise source.

Throughout this work we consider the following Ohmic spectral density function with exponential cut-off

$$J(\omega) = M\gamma\omega \exp(-\omega/\omega_C), \quad (4)$$

where $\omega_C \gg \omega_0$.

In the quantum Langevin equation for the model, the parameter γ is the frequency independent damping constant. Correspondingly, the Langevin equation features a memoryless damping kernel and therefore, in the classical limit, the bath considered reduces to a white noise source. By comparing the discrete and the continuous version of $J(\omega)$, one can recognize that the damping constant γ is a measure of the overall coupling strength between the particle and the bath.

B. The two-level system

If the particle is initially in a superposition of the two lower energy states ($|g\rangle, |e\rangle$) of the potential $V(q)$, and the temperature is low enough, to a good approximation the system can be considered a TLS and the model in Eq. (1) reduces to the celebrated *spin-boson* (SB) model [16]. A picture of the TLS dynamics in terms of tunneling from one well to the other is given by the localized basis, where the left/right well states $|R/L\rangle$ are combinations of $|g\rangle$ and $|e\rangle$. In the localized basis the free TLS Hamiltonian reads

$$\hat{H}_{TLS} = -\frac{\hbar}{2}(\Delta\sigma_x + \epsilon\sigma_z), \quad (5)$$

where Δ is the tunneling frequency, ϵ is the (static) bias. The spin operators in the localized basis are $\sigma_z = |R\rangle\langle R| - |L\rangle\langle L|$ and $\sigma_x = |R\rangle\langle L| + |L\rangle\langle R|$.

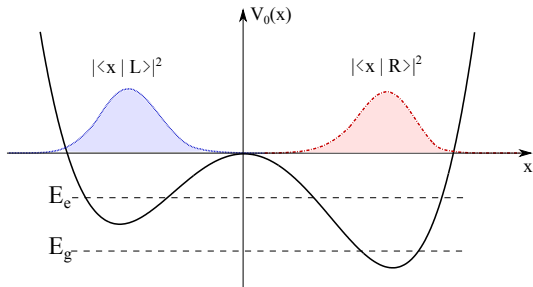


FIG. 1. (Color online) Asymmetric double well potential and probability densities relative to the localized basis states $\{|L\rangle, |R\rangle\}$ for the two level system. The energy separation is $E_e - E_g = \hbar\sqrt{\epsilon^2 + \Delta^2}$ (see. Eq. (5)).

For the SB dynamics there exist various approximation schemes. When the system is weakly coupled to the heat bath (usually this is the case for quantum optical systems and qubit setups), the approach traditionally used is that of a Born-Markov master equation for the system's RDM [24]. It captures well the coherent tunneling dynamics, characterized by the relaxation and dephasing rates $\Gamma_{rel} = \tau_1^{-1}$ and $\Gamma_{ph} = \tau_2^{-1}$, respectively.

However, the perturbative in the coupling character of this approach makes it unsuited in situations where the coupling is not weak. In this case the real-time path integral techniques can be used to trace out the bath degrees of freedom and obtain a still exact formal expression for the RDM. This expression can, in some cases, be numerically evaluated by tensor multiplication [25] or using Monte Carlo or stochastic techniques [26–29]. However, the numerical evaluation of the path integral is a hard task, especially at long times.

It is therefore convenient to have an equation for the RDM in the form of the Nakajima-Zwanzig equation [30], which captures the non-Markovian reduced dynamics of a general system plus bath model. The difficult task, in this case, is to have a reasonably simple expression for the kernel.

Starting from the real-time path integral expression for the particle's RDM, there are different approximation schemes, all yielding a generalized (integro-differential) master equation for the populations in a spatially localized representation. By tracing out the bath degrees of freedom, the amplitude associated to a path has the factorized form of a bare amplitude, relative to the free system, multiplied by the Feynman-Vernon (FV) influence functional [21]. This weights the path according to the effect exerted by the particle's motion on the bath degrees of freedom.

The FV influence introduces nonlocal in time correlations inside the paths which make the path integral expression intractable when the confining potential is

anharmonic. For the SB dynamics the simplest, non-perturbative in the coupling approximation is the non-interacting blip approximation (NIBA) [16]. The NIBA scheme neglects the nonlocal part of the correlations due to an exponential cutoff in the FV functional, which is effective at high temperature and/or strong damping. This approach, while being non-perturbative in the coupling, is perturbative in the tunneling Δ .

In the opposite damping regime, the weak coupling approximation (WCA) [31], treating the coupling to the first order and Δ to all orders, is appropriate. It gives the same results as the Born-Markov approach. Finally, an approach exists which interpolates between these two extrema by considering the local correlations fully and the nonlocal ones to the first order in the coupling. This scheme is called weakly interacting blip approximation (WIBA) [32], and, by construction, also covers the intricate regime of intermediate temperatures and damping, where both the WCA and the NIBA fail.

However, beyond the TLS approximation, this crossover regime is not accessible to currently existing Bloch-Redfield-like [19, 20] or NIBA-like [4, 5] approximation schemes.

In this work we consider a generalization of the SB model to a four level bistable system, the so-called double-doublet system (DDS), because its energy levels are arranged in well separated doublets due to the strong nonlinearity of the potential (see Fig. 2). Basing on a difference in time-scales between the fast intra-well motion and the slow inter-well (tunneling) dynamics, we treat the first according to the WIBA scheme and the second according to the NIBA. The resulting scheme covers the crossover region of intermediate temperatures and damping in the parameter space of the dissipative DDS.

C. The double-doublet system

Including successive energy states beyond the first two, a *localized* basis can still be constructed, as for the TLS (see Fig. 1), with a unitary operation on the energy eigenbasis. The resulting discrete variable representation (DVR) [33] is the one in which the particle's position operator is diagonal

$$\hat{q}|Q_j\rangle = Q_j|Q_j\rangle. \quad (6)$$

In Fig. 2 the energy and the DVR eigenstates are shown for the specific four-state system considered in this work, i.e. the symmetric double well potential ($\epsilon = 0$ in Eq. (2)) with the relevant Hilbert space spanned by the first four energy eigenstates. Since the corresponding energy levels are arranged in a pair of two well separated doublets, the system is called double-doublet system (DDS).

The doublets are characterized by internal frequency differences $\Omega_2 \ll \Omega_1 \ll \Omega_0$, where $\hbar\Omega_2 = E_2 - E_1$ and $\hbar\Omega_1 = E_4 - E_3$ are the intra-doublet (or tunneling) splittings, and $\hbar\Omega_0 = (E_4 + E_3)/2 - (E_2 + E_1)/2$ is the average inter-doublet spacing, which is of the order of $\hbar\omega_0$.

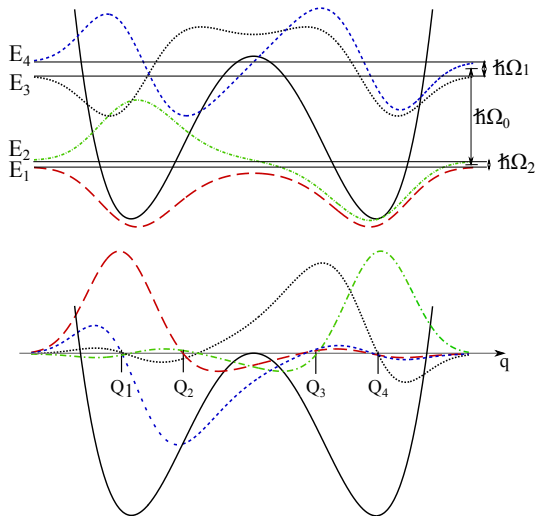


FIG. 2. (Color online) Potential V (Eq. (2)) with $\Delta U = 1.4\hbar\omega_0$ and $\epsilon = 0$. The minima are at $q_{L/R} \mp 3.35\sqrt{\hbar/(M\omega_0)}$. *Upper panel* - The four energy levels (horizontal lines) and the respective energy eigenfunctions. The spacing between the first two levels is exaggerated for the sake of clarity. The frequency $\Omega_0 = 0.8151\omega_0$ is the average inter-doublet frequency spacing while the tunneling frequency splittings of the higher and the lower doublet are $\Omega_1 = 0.1212\omega_0$ and $\Omega_2 = 0.0037\omega_0$, respectively. *Lower panel* - The four DVR position eigenvalues (vertical lines) and the corresponding DVR eigenstates.

The numerical values for the potential used in this work are given in Fig. 2. The DVR basis set is composed by the four functions shown in the lower panel of Fig. 2. They are peaked around the four eigenvalues Q_1, \dots, Q_4 so that for the particle to be in the state $|Q_j\rangle$ means to be *localized* around Q_j .

It is important to notice that limiting the energy levels involved in the system dynamics to the first four is a good approximation as long as the environment is not likely to excite the particle to higher energies, i.e. as long as $k_B T/\hbar \lesssim \Omega_0$.

The free DDS dynamics is shown in Fig. 3 considering the system initially in the state

$$|Q_1\rangle = \frac{v}{\sqrt{2}}(|1\rangle - |2\rangle - u|3\rangle + u|4\rangle), \quad (7)$$

where $v = (1 + u^2)^{-1/2}$ and $u \simeq -0.585$. Initial condition (7) involves all of the four energy states spanning the Hilbert space of the DDS. The resulting dynamics highlights all of the three relevant time scales of the problem.

In the upper panel of Fig. 3 a comparison is made between the time evolution of left well population $P_L^{DDS} = \rho_{11} + \rho_{22}$ of the DDS, starting in the state (7), and the corresponding quantity, P_L^{TLS} , for the same system in the TLS approximation, starting in the state $|L\rangle$ (see Fig. 1).

Contrary to the TLS dynamics, characterized by a single frequency, the dynamics of the free DDS displays

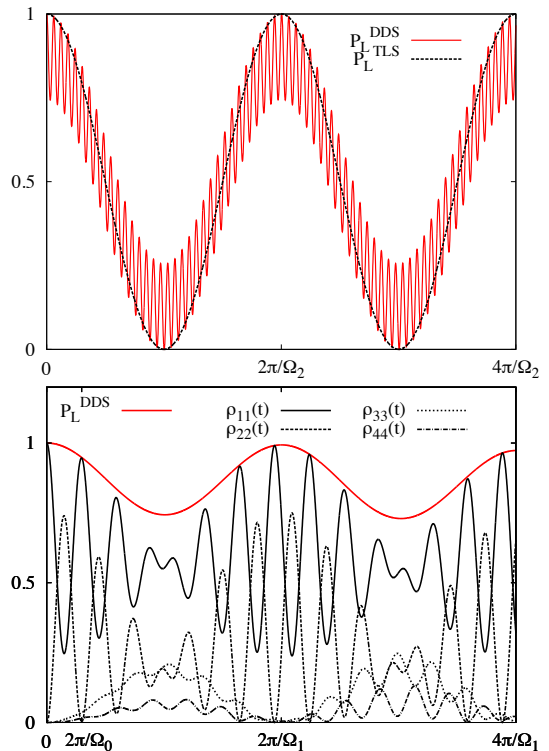


FIG. 3. (Color online) Time evolution of the populations in the DVR for the free DDS with initial condition $\rho(t_0 = 0) = |Q_1\rangle\langle Q_1|$ (analytical result). *Upper panel* - Long time dynamics of the left well population $P_L = \rho_{11} + \rho_{22}$ compared to the $|L\rangle$ state population of the system in the TLS approximation. *Lower panel* - Short time dynamics of the left well population of the DDS and time evolution of the single populations of the DVR basis states.

fast intra-well oscillations of frequency Ω_0 and a tunneling dynamics, occurring at two distinct time scales: the shorter one is given by the higher energy doublet (frequency Ω_1 , see Fig. 2) and the longer one occurs on the timescale set by the smallest characteristic frequency $\Omega_2 = (E_2 - E_1)/\hbar$. As shown in Fig. 3, the long time oscillations coincide with those of the system in the TLS approximation starting with the particle in the left well. The rich dynamics described reflects the configuration of the energy levels in two well separated doublets (see Fig. 2), with different inter-doublet separation, and allows for the approximations on the Feynman-Vernon influence functional which will be introduced in Sec. IV.

Before going into the details of the path integral approach applied to the dissipative dynamics of the DDS, it is appropriate to discuss the role of the initial condition in determining, along with the dissipation regime, the validity of the TLS approximation. This is done in the next section.

D. Initial preparation and the validity of the TLS approximation

At low temperature ($k_B T \ll \hbar \Omega_0$) the TLS approximation is appropriate and yields the same predictions as those obtained considering higher energy states, provided that no energy levels other than the first two are involved in the initial preparation¹.

This is exemplified in Fig. 4 where, at weak damping and low temperature, the time evolution of the left well population of the TLS, initially in the state $|L\rangle$, is compared with the left well population of the DDS prepared in the state

$$|L\rangle_{TLS} = v(|Q_1\rangle - u|Q_2\rangle) = (|1\rangle + |2\rangle)/\sqrt{2}. \quad (8)$$

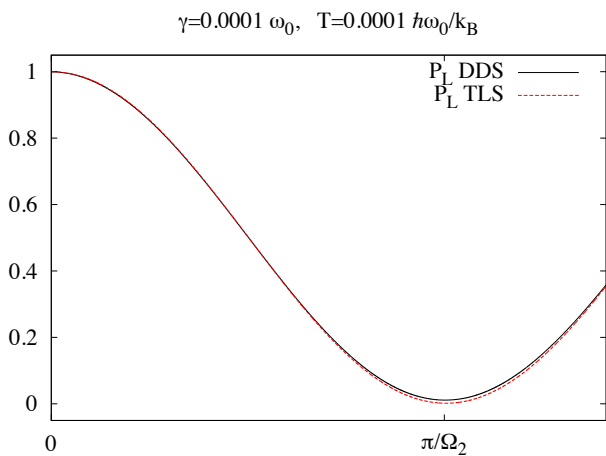


FIG. 4. (Color online) Comparison between the time evolution of $P_L^{DDS} = \rho_{11} + \rho_{22}$ of DDS in the regime of validity of the TLS approximation with initial condition given in Eq. (8) and P_L^{TLS} for the TLS initially in the state $|L\rangle$. Both results are obtained by the Bloch-Redfield master equation approach.

In the dissipation regime considered in Fig. 4, our system is well described by the (perturbative in the coupling) technique of the Bloch-Redfield master equation, which is derived starting from the microscopic model described in Sec. II A, under the assumptions that the coupling is weak and the correlation time of the environment is much shorter than the dynamical time scales (Born-Markov approximation). In the resulting picture no influence on the environment is exerted by the particle and consequently no back-action from the environment affects the system's evolution. This gives the Markovian master equation for the RDM in the energy representation

$$\dot{\rho}_{nm}^E(t) = -i\omega_{nm}\rho_{nm}^E(t) + \sum_{k,l} \mathcal{L}_{nm,kl} \rho_{kl}^E(t), \quad (9)$$

¹ This is not generally true for a driven system.

whose analytical solution is discussed in Appendix C. This master equation is characterized by the so-called dephasing rates $|\mathcal{L}_{ij,ij}|$, fixing the coherence time of a superposition of energy states E_i and E_j , or, in the space localized description of the DVR, the time scale of decay of an oscillatory behavior of frequency $\omega_{ij} = \omega_i - \omega_j$. Due to its perturbative character, the Bloch-Redfield approach fails in the intermediate to strong coupling regime and the path integral approach, introduced in Sec. III, has to be used.

The Bloch-Redfield approach, applied to the DDS with initial condition (8) and to the TLS starting in the state $|L\rangle$, gives, as expected, the same behavior for P_L^{DDS} and P_L^{TLS} (see Fig. 4).

However, if the initial preparation of the DDS involves the second energy doublet, the behavior of the DDS differs dramatically from that of the TLS, even at zero temperature, in a similar way to that shown by the comparison made in Fig. 3.

In the next section, along the line of Ref. [5], a formally exact expression for the RDM of our four-level system, in the basis of Eq. (6), is derived. Approximations which go beyond the generalized NIBA (gNIBA) proposed in Ref. [5] are discussed in Sec. IV. Notice that the parameters of the bistable potential are chosen as in [5], such that some of the results presented there for the incoherent regime can be used as reference.

III. PATH INTEGRAL APPROACH

Let \mathcal{W} be the full system-plus-reservoir density matrix at time t . Its time evolution is given by

$$\mathcal{W}(t) = U(t, t_0)\mathcal{W}(t_0)U^\dagger(t, t_0)$$

where $U(t, t_0) = \exp(-i\hat{H}(t - t_0)/\hbar)$, \hat{H} being the full Hamiltonian of Eq. (1). To calculate the system's dynamics when the system-bath coupling γ is not weak, we cannot make use of techniques perturbative in γ , such as the Born-Markov master equation approach [17].

To this extent we use rather the path integral approach which, being inherently non-perturbative in γ , has been proven useful to treat cases of strong as well as of weak dissipation [14]. Within this approach, the elements of the RDM in the position representation

$$\rho_{qq'}(t) = \langle q|Tr_B \mathcal{W}(t)|q'\rangle$$

(where Tr_B indicates the trace over the bath's degrees of freedom) are the dynamical objects of interest. Assuming a factorized initial condition, with the particle prepared in the state $\rho(t_0)$ and the bath initially in the thermal state $R^{Th} = Z^{-1} \exp(-\beta \hat{H}_B^E)$, i.e.

$$\mathcal{W}(t_0) = \rho(t_0) \otimes R^{Th}, \quad (10)$$

the particle's reduced density matrix at time t , in the position representation, is given by

$$\rho_{qq'}(t) = \int dq_0 \int dq'_0 G(q, q', t; q_0, q'_0, t_0) \rho_{q_0 q'_0}(t_0). \quad (11)$$

The propagator for the density matrix has the form of a double path integral

$$G(q, q', t; q_0, q'_0, t_0) = \int_{q(t_0)=q_0}^{q(t)=q} \mathcal{D}q \int_{q'(t_0)=q'_0}^{q'(t)=q'} \mathcal{D}^* q' e^{\frac{i}{\hbar}(S[q]-S[q'])} \mathcal{F}_{FV}[q, q'] \quad (12)$$

where, denoting by $\mathbf{x}(t)$ the collective position coordinate of the bath at time t , the FV influence functional reads

$$\mathcal{F}_{FV}[q, q'] = \int d\mathbf{x}_0 d\mathbf{x}'_0 R_{\mathbf{x}_0 \mathbf{x}'_0}^{Th} \int d\mathbf{x} \times \int_{\mathbf{x}(t_0)=\mathbf{x}_0}^{\mathbf{x}(t)=\mathbf{x}} \mathcal{D}\mathbf{x} \int_{\mathbf{x}'(t_0)=\mathbf{x}'_0}^{\mathbf{x}'(t)=\mathbf{x}} \mathcal{D}^* \mathbf{x}' e^{\frac{i}{\hbar}(S[q, \mathbf{x}]-S[q', \mathbf{x}'])}. \quad (13)$$

In these path integral expressions, the action functional $S[q(\tau)]$ for the bare system (particle in the potential V) is

$$S[q] = \int_{t_0}^t dt' \left(\frac{p^2(t')}{2M} - V(q(t')) \right)$$

and the action functional $S[q(\tau), \mathbf{x}(\tau)]$ of the bath oscillators subject to the influence of the particle's motion is

$$S[q, \mathbf{x}] = \frac{1}{2} \sum_{j=1}^N \int_{t_0}^t dt' \left[\frac{p_j^2(t')}{m_j} - m_j \omega_j^2 \left(x_j(t') - \frac{c_j}{m_j \omega_j^2} q(t') \right)^2 \right].$$

The path integral for the bath oscillators can be solved analytically, being a set of Gaussian integrals. Setting

$$\mathcal{F}_{FV} = \exp(-\Phi_{FV}), \quad (14)$$

the influence phase functional Φ_{FV} takes the form

$$\begin{aligned} \Phi_{FV}[y, x] &= \frac{1}{\hbar^2} \int_{t_0}^t dt' \int_{t_0}^{t'} dt'' y(t'') \\ &\times [L'(t' - t'')y(t'') + iL''(t' - t'')x(t'')] \\ &+ i \frac{\mu}{2\hbar^2} \int_{t_0}^t dt' x(t')y(t'), \end{aligned} \quad (15)$$

where we have introduced the relative and center of mass coordinates

$$y(t) = q(t) - q'(t) \quad \text{and} \quad x(t) = q(t) + q'(t).$$

Finally, $L(t)$ is the bath force correlation function

$$\begin{aligned} L(t) &= L'(t) + iL''(t) \\ &= \frac{\hbar}{\pi} \int_0^\infty d\omega J(\omega) \left(\coth \frac{\hbar\omega\beta}{2} \cos \omega t - i \sin \omega t \right) \end{aligned} \quad (16)$$

and $\mu = 2\hbar/\pi \int_0^\infty d\omega J(\omega)/\omega$ [14]. If the particle is free or subject to a harmonic potential, the path integral in Eq. (12) can be evaluated analytically [34]. In our case, the nonlinearity of the double well potential does not allow for an exact evaluation of $\rho_{qq'}(t)$ and approximations are required.

A. Exact reduced density matrix in the DVR

In the spatially discretized picture for the DDS discussed in Sec. II C, the double path $(q(t), q'(t))$ is no more a continuous function of time but a walk on a two-dimensional spatial grid with 4×4 grid-points. Each coordinate takes values in the set $\{Q_1, \dots, Q_4\}$. The path integral in Eq. (12) turns into a sum over all the possible path configurations, integrated over the transition times. An example of double path with five transitions is shown in Fig. 5.

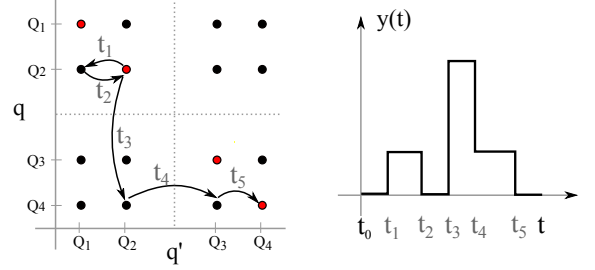


FIG. 5. (Color online) *Left panel* - Example of a double path in the DVR plane (q, q') in which the two diagonal sites (Q_2, Q_2) and (Q_4, Q_4) are connected by five transitions. When the path crosses the horizontal (vertical) dotted line the coordinate q (q') is making a tunneling transition. *Right panel* - Time resolved picture of the path in the left panel in terms of relative coordinate $y = q - q'$. The path has three sojourns and two clusters.

The discretized version of Eq. (11) is

$$\rho_{qq'}(t) = \sum_{q_0, q'_0=Q_1}^{Q_4} G(q, q', t; q_0, q'_0, t_0) \rho_{q_0 q'_0}(t_0), \quad (17)$$

with the propagator in the form of the double dissipative path integral

$$G(q, q', t; q_0, q'_0, t_0) = \sum_{n=0}^{\infty} \int_{t_0}^t D_n \{t_j\} \mathcal{A}(q) \mathcal{A}^*(q') \mathcal{F}_{FV}(x, y). \quad (18)$$

The symbol $\int_{t_0}^t D_n \{t_j\}$ indicates

$$\int_{t_0}^t D_n \{t_j\} = \sum_{\text{paths}_n} \int_{t_0}^t dt_n \int_{t_0}^{t_n} dt_{n-1} \dots \int_{t_0}^{t_2} dt_1. \quad (19)$$

Here the summation is over all of the possible sets of n couples of coordinates (q_j, q'_j) , i.e. over all the double discretized paths with n transitions, starting at (q_0, q'_0) and ending at (q, q') , see Fig. 5. The bare amplitude for one of these paths is given by

$$\mathcal{A}(q) \mathcal{A}^*(q') = B_0(t_1 - t_0) \prod_{j=1}^n (-i) \Delta_j B_j(t_{j+1} - t_j), \quad (20)$$

where we set $t_{n+1} \equiv t$. The q/q' transition amplitudes per unit time are defined by

$$\Delta_j = \begin{cases} \frac{1}{\hbar} \langle q_j | \hat{H}_S | q_{j-1} \rangle & \text{for a } q \text{ transition} \\ -\frac{1}{\hbar} \langle q'_j | \hat{H}_S | q'_{j-1} \rangle & \text{for a } q' \text{ transition} \end{cases} \quad (21)$$

and the *bias factors* by

$$B_j(t_{j+1} - t_j) = \exp[-i\epsilon_j(t_{j+1} - t_j)], \quad (22)$$

where

$$\epsilon_j = \frac{1}{\hbar} \left(\langle q_j | \hat{H}_S | q_j \rangle - \langle q'_j | \hat{H}_S | q'_j \rangle \right). \quad (23)$$

The factors Δ_j and ϵ_j are the multi-state generalizations of the tunneling element and bias in the TLS Hamiltonian (Eq. (5)).

We list their values, for the symmetric DDS, using two indexes to specify the states q_j and q'_j , whereas in Eqs. (21) and (23) the single index specifies the transition number. In terms of the frequency differences $\omega_{ij} = \omega_i - \omega_j = (E_i - E_j)/\hbar$ and of the constant u , which depends on the parameters of the potential ($u \simeq -0.585$ in our problem), the Δ are given by

$$\begin{aligned} \Delta_{12} &= \Delta_{21} = -\Delta_{43} = -\Delta_{34} = v^2 u \Omega_0, \\ \Delta_{13} &= \Delta_{31} = -\Delta_{24} = -\Delta_{42} = \frac{v^2 u}{2} (\omega_{43} - \omega_{21}), \\ \Delta_{23} &= \Delta_{32} = \frac{v^2}{2} (\omega_{43} + u^2 \omega_{21}), \\ \Delta_{14} &= \Delta_{41} = \frac{v^2}{2} (u^2 \omega_{43} + \omega_{21}), \end{aligned} \quad (24)$$

and the biases

$$\begin{aligned} \epsilon_{12} &= \epsilon_{13} = \epsilon_{43} = \epsilon_{42} = -\epsilon_{21} = -\epsilon_{41} = -\epsilon_{34} = -\epsilon_{24} \\ &= v^2 (u^2 - 1) \Omega_0, \\ \epsilon_{14} &= \epsilon_{41} = \epsilon_{23} = \epsilon_{32} = 0, \end{aligned} \quad (25)$$

where $v = (1 + u^2)^{-1/2}$. The last line of Eq. (25) derives from the symmetry of the problem.

In the DVR, the phase of the Feynman-Vernon (FV) influence functional (Eq. (14)) turns into

$$\Phi(\xi, \chi)_{FV} = - \sum_{i=1}^n \sum_{j=0}^{i-1} (\xi_i Q'_{ij} \xi_j + i \xi_i Q''_{ij} \chi_j) \quad (26)$$

where

$$\begin{aligned} \xi_j &= y_j - y_{j-1} = q_j - q'_j - q_{j-1} + q'_{j-1}, \\ \chi_j &= x_j - x_{j-1} = q_j + q'_j - q_{j-1} - q'_{j-1} \end{aligned}$$

are the so-called *charges*. The shorthand notation Q'_{ij} and Q''_{ij} in Eq. (26) stands for $Q'(t_i - t_j)$ and $Q''(t_i - t_j)$, respectively. The function $Q(t) = Q'(t) + iQ''(t)$ is related to the bath force correlation function by $L(t)/\hbar^2 = d^2 Q(t)/dt^2$ (see Eq. (16)).

In what follows we use the Ohmic spectral density function with exponential cutoff $J(\omega) = M\gamma\omega \exp(-\omega/\omega_C)$, where $\omega_C \gg \omega_0$. With this choice and in the limit ($\hbar\omega_C \gg k_B T$) the function $Q(t)$ has the form

$$\begin{aligned} Q(t) &= \frac{M\gamma}{\pi\hbar} \ln \left(\sqrt{1 + \omega_C^2 t^2} \frac{\sinh(\kappa t)}{\kappa t} \right) \\ &\quad + i \frac{M\gamma}{\pi\hbar} \arctan(\omega_C t), \end{aligned} \quad (27)$$

where $\kappa = \pi k_B T / \hbar$.

IV. APPROXIMATIONS

We want to study the DDS dissipative dynamics in terms of the time evolution of the populations, the diagonal elements of the RDM in the DVR basis, assuming that the particle is initially in the state $|Q_1\rangle$. This amounts to calculate the propagator (see Eq. (17))

$$\rho_{kk}(t) = G(Q_k, Q_k, t; Q_1, Q_1, t_0), \quad k = 1, \dots, 4. \quad (28)$$

The evaluation of the propagator involves two main difficulties. The first one is that, contrary to the TLS case, the variety of possible paths of the multi-state system makes the summation difficult, if not impossible, even in the absence of coupling with the bath. This feature calls for a selection on the paths to be summed.

The second difficulty is constituted by the intricate set of time nonlocal correlations among the ξ_i and χ_j charges, introduced by \mathcal{F}_{FV} , which make the path integral expression intractable.

Hereinafter we shall use an approximation on \mathcal{F}_{FV} which is based on the separation of time scales between the *intra-well* and the *inter-well* dynamics. The first one is characterized by transitions among states in the same well, called *vibrational relaxation* events (VR). The inter-well dynamics consists of transitions among states in different wells, called tunneling events (T).

A. Selection on the paths and retained interactions

When a double path is in a diagonal configuration ($q = q'$), it is said to be in a *sojourn*. The non-diagonal configuration ($q \neq q'$) between two consecutive sojourns forms a *cluster*. The latter is a generalization of the *blip* configuration for the TLS [16]. The difference is that a blip consists, for geometrical reasons, of a single off-diagonal excursion while a cluster can be made of an arbitrary long sequence of off-diagonal transitions. In Fig. 5 we give an example of a path with three sojourns and two clusters, the first of which is a simple blip and the second a proper cluster with multiple off-diagonal excursions.

For Ohmic damping with exponential cutoff at a high frequency ω_C , the long time or high temperature limit

($t \gg \hbar/k_B T$) of the bath correlation function (Eq. (27)) is

$$Q(t) = \frac{M\gamma}{\pi\hbar} \left[\kappa t - \ln \left(\frac{2\kappa}{\omega_C} \right) \right] + i \frac{M\gamma}{2\hbar}, \quad (29)$$

where $\kappa = \pi k_B T / \hbar$. In this limit, the inter-cluster interactions cancel out exactly, so that the suppression of the path weight exerted through $Q'(t)$ depends on the length of the cluster. For this reason, in the presence of the dissipative Ohmic environment considered here, the contribution of paths with long off-diagonal excursions is suppressed. Thus, the main contribution to the sum (18) is given by those path returning in a sojourn after a single off-diagonal excursion.

The first approximation we do is to consider only this class of paths. Following the TLS convention, we call the off-diagonal configurations *vibrational relaxation-blips* (VR-blips), if q and q' belong to the same well, and *tunneling-blips* (T-blips), if q and q' belong to different wells.

The second approximation consists in neglecting, among the interactions induced by \mathcal{F}_{FV} , i) all the interactions between couples of T-blips, ii) those between a T-blip and a VR-blip and iii) the interactions between two non-consecutive VR-blips. This approximation is justified by the long time scale of the tunneling dynamics, i.e. by the fact that, on the average, tunneling events are rare, because the transition amplitude per unit time associated with them is small in comparison with that of a VR event. Since in a typical path the T-blips are well separated in time, their ξ and χ charges interact through the long time limit of the bath correlation function, meaning that the total interaction sums up to zero, as stated above.

Moreover, a tunneling blip is strongly suppressed by the environment, since $\xi_j \xi_{j-1} = -(q_j - q'_j)^2$ in Eq. (26) is large if q and q' are in different wells. The resulting picture, for a typical path among those retained in the summation, is that of a sequences of frequent VR-blips, which we call **VR-blip chain**, interrupted by T-blips, as sketched in Fig. 6. Notice that, inside a VR-blip chain, the interactions are retained.

Under these two approximations the system decouples into a set of six TLSs. Any double path can be seen as a sequence of arbitrarily long, non-interacting paths inside the two dimensional sublattices in Fig. 7. Each of these sublattices represents a different TLS characterized by its own bias factor, tunneling element and distance between the spatial coordinates.

B. Weakly-interacting VR-blip approximation

The approximations done still allow for the treatment of the VR-blip chains, i.e. the motion of the TLSs formed by the couples of states inside each well, to arbitrary accuracy.

Again, also for an intra-well TLS, an exact treatment

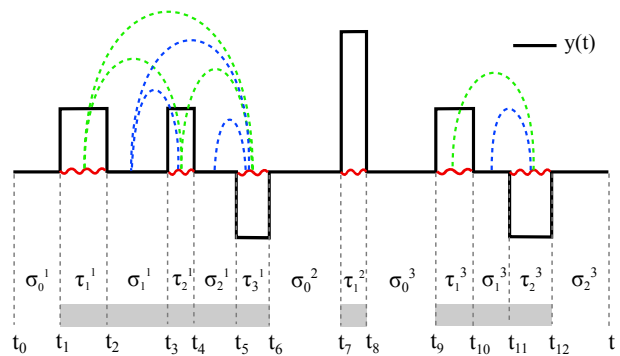


FIG. 6. (Color online) A path made by two VR-blip chains separated by a T-blip. The transition times and the blip/sojourn times are indicated. The shaded areas on the lower part of the figure represent the time intervals inside which the correlations are retained according to the approximations discussed in Sec. IV A. Specifically, according to the VR-WIBA scheme introduced in Sec. IV B, the intra-VR-blip and intra-T-blip interactions (solid wavy lines) are taken at all order in γ while the inter-VR-blip and VR-blip-sojourn interactions (dashed lines) are taken to the first order in γ .

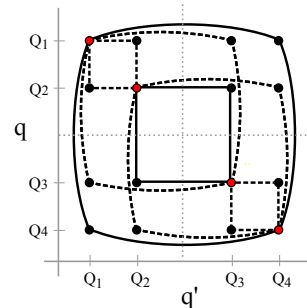


FIG. 7. (Color online) With the limitations on the allowed paths and the separation of the intra- and inter-well dynamics, the motion of the system in the 4×4 grid of spatial positions decouples into a sequence of arbitrarily long paths inside the six two-dimensional square sublattices in the figure, each one representing a different TLS. The dashed squares indicate the TLSs with nonzero effective bias while the solid squares indicate symmetric TLSs.

is impossible due to the intricacies brought by \mathcal{F}_{FV} . It is therefore necessary to make further approximations on the nonlocal interactions inside the VR-blip chains. At high temperatures, in the limits of the DDS description, the long time limit of $Q(t)$ (see Eq. (29)) is attained at short times. If the linearized form is attained on time scales of the order of magnitude of the average separation between two VR-blips, they can be considered noninteracting objects. This amounts to retain only the local in time effects introduced by \mathcal{F}_{FV} . The resulting scheme for the intra-well dynamics is the well known NIBA. Within the NIBA for the VR-blip chains every blip is nonin-

interacting with any other. The resulting overall scheme is the multi-level generalization of the NIBA, which can be called generalized non-interacting blip approximation (**gNIBA**)².

At lower temperature the gNIBA breaks down because the inter-blip interactions are not removed completely inside a VR-blip chain. However, due to the long time scale of the inter-well dynamics, the isolation of the T-blips is still valid if the cutoff operated by \mathcal{F}_{FV} occurs on the time scale Ω_1^{-1} of the fast tunneling dynamics.

To account for inter-blip correlations in the VR dynamics, we adapt to our purposes a scheme for the TLS, called *weakly interacting blip approximation* (WIBA) [32], which interpolates between strong and weak damping regimes. The scheme retains, to the first order in γ , the nonlocal part of the interactions among the VR-blips and, to all orders, the interactions inside the VR-blips. We name the resulting overall scheme for the DDS **VR-WIBA** [35].

From what stated above two considerations can be made about the validity of our VR-WIBA approximation scheme. The first is that the region of the parameter space in which the VR-WIBA is valid includes that of the gNIBA, because the isolation of any blip implies the separation among T-blips and VR-blip chains. The second comment is that, while the validity of the gNIBA is established by the temperature and depends weakly on the damping, in determining the validity of the VR-WIBA both temperature and damping play an important role.

In the Sec. V we discuss in more detail the validity domains and in Sec. VI we show and compare their results for the dissipative DDS dynamics.

C. VR-WIBA generalized master equation

By properly taking into account the above approximations every double path can be considered as a sequence of non-interacting paths along the two 2×2 sublattices in Fig 7. A sublattice is identified by the coordinates of two diagonal sites (red dots in the figure). Suppose a sublattice has diagonal sites (q_A, q_A) and (q_B, q_B) . Then the path inside this sublattice is mapped onto the motion of the TLS $\{|q_A\rangle, |q_B\rangle\}$. Every TLS path has, by definition, an even number of transitions, since it starts and ends in a diagonal configuration, so the whole path has an even number $2n$ of transitions (see Fig. 7). We can therefore factorize the amplitude $A(t_0, \dots, t_{2n}, t) = \mathcal{A}(q)\mathcal{A}^*(q')\mathcal{F}_{FV}(x, y)$ into the product of the amplitudes A_j associated to the paths into the TLSs. The initial and final states are fixed: $q_0 = Q_1$ and $q_n = Q_k$.

From inspection of equations (20) and (26) (see also

Fig. 6) we see that the amplitudes do not depend on the last sojourn time.

Moreover we neglect, in each of the amplitudes A_j , the interactions involving the first sojourn time (this is justified by the fact that the VR-blip chains and the T-blips are well separated, which implies a long first sojourn time).

If a path switches among different sublattice M times, with $2k_j$ transitions in the j -th sublattice and $\sum_{j=1}^N k_j = n$, we have

$$A(t_1, t_2, \dots, t_{2n-1}, t_{2n}) = \prod_{j=1}^M A_j(\tau_1^j, \sigma_1^j, \dots, \sigma_{k_j-1}^j, \tau_{k_j}^j), \quad (30)$$

where $\tau_j = t_{2j} - t_{2j-1}$ are the blip times and $\sigma_j = t_{2j+1} - t_{2j}$ the sojourn times.

The population $\rho_{kk}(t)$ of the state $|Q_k\rangle$ at time t , given the initial condition $\rho(t_0) = |Q_1\rangle\langle Q_1|$ (see Eq. (28)), is

$$\rho_{kk}(t) = \delta_{Q_k Q_1} + \sum_{n=1}^{\infty} \int_{t_0}^t \mathcal{D}_{2n}\{t_j\} A(t_0, t_1, \dots, t_{2n}, t). \quad (31)$$

Due to the fact that the amplitudes in this sum over the paths factorize as in Eq. (30), the Laplace transform of $\rho_{kk}(t)$ reads

$$\rho_{kk}(\lambda) = \frac{\delta_{Q_k Q_1}}{\lambda} + \frac{1}{\lambda} \sum_{M=1}^{\infty} \sum_{\{q_j\}=Q_1}^{Q_4} \prod_{j=1}^M \frac{\hat{K}_{q_{j-1}q_j}(\lambda)}{\lambda}, \quad (32)$$

where, for $q_j \neq q_{j-1}$, the functions $\hat{K}_{q_{j-1}q_j}(\lambda)$ are the Laplace transforms of the TLS kernel $K_{q_{j-1}q_j}(\tau)$ in the master equation for the populations of the TLS $\{|q_{j-1}\rangle, |q_j\rangle\}$ (see Appendix A).

We now switch to vector notation. We define the four-dimensional vector $\vec{\rho}(\lambda)$, whose components are the Laplace transform $\rho_{kk}(\lambda)$ of the four populations. Defining also the 4×4 matrix $\hat{\mathcal{K}}(\lambda)$, whose elements are the functions $\hat{K}_{q_j q_{j-1}}(\lambda)$, Eq. (32) reads

$$\begin{aligned} \vec{\rho}(\lambda) &= \frac{\vec{\rho}(t_0)}{\lambda} + \frac{1}{\lambda} \sum_{M=1}^{\infty} \left[\frac{\hat{\mathcal{K}}(\lambda)}{\lambda} \right]^M \vec{\rho}(t_0) \\ &= \frac{1}{\lambda} \sum_{N=0}^{\infty} \left[\frac{\hat{\mathcal{K}}(\lambda)}{\lambda} \right]^N \vec{\rho}(t_0) \\ &= \left[\lambda \mathbb{I} - \hat{\mathcal{K}}(\lambda) \right]^{-1} \vec{\rho}(t_0). \end{aligned} \quad (33)$$

Transforming back to the time domain we obtain the following generalized master equation (GME)

$$\dot{\vec{\rho}}(t) = \int_{t_0}^t dt' \mathcal{K}(t-t') \vec{\rho}(t'),$$

where $\mathcal{K}(t) = \mathcal{L}^{-1}\{\hat{\mathcal{K}}(\lambda)\}$. Restoring the index notation, we find equivalently

$$\dot{\rho}_{kk}(t) = \sum_{j=1}^4 \int_{t_0}^t dt' K_{kj}(t-t') \rho_{jj}(t'). \quad (34)$$

² This scheme corresponds to the generalized non-interacting cluster approximation (gNICA) at the leading order in the Δ factors [5].

The diagonal elements of the kernel matrix $\mathcal{K}(t)$ are given by the probability conservation

$$K_{jj}(t) = - \sum_{i(\neq j)=1}^4 K_{ij}(t).$$

The non-diagonal elements have been defined as the TLS kernels corresponding to the motion into the sublattices. These elements of the kernel matrix are taken within different approximation schemes, according to the populations they connect in the GME. Specifically, on the basis of the approximations made, they are classified as follows

- If the DVR states k and j belong to different wells, i.e. $(k, j) = (1, 3), (3, 1), (1, 4), (4, 1), (2, 3), (3, 2), (2, 4), (4, 2)$, the corresponding kernel is a NIBA kernel $K_{kj}^N(t)$.
- If the DVR states k and j belong to the same well, i.e. $(k, j) = (1, 2), (2, 1), (3, 4), (4, 3)$, the nonlocal correlations can be, in principle, taken into account to any accuracy. We use the WIBA scheme for these intra-well kernels. In this scheme they consist of a NIBA plus a beyond-NIBA part

$$K_{kj}^W(t) = K_{kj}^N(t) + K_{kj}^{BN}(t).$$

If we set to zero the beyond-NIBA correction in these *intra-well kernels* we obtain the gNIBA scheme for the DDS discussed in Ref. [4].

The explicit expressions for the kernels are given in Appendix B.

At strong damping, in the incoherent regime (see Sec. V), the populations evolve on time scales larger than the time intervals over which the gNIBA kernels are substantially different from zero. This observation suggests that it is appropriate to cast the gNIBA GME into the Markov approximate master equation form

$$\dot{\rho}_{kk}(t) = \sum_{j=1}^4 \Gamma_{ij} \rho_{jj}(t), \quad (35)$$

where

$$\Gamma_{ij} = \int_0^\infty dt K_{kj}^{gN}(t).$$

Equation (35) admits the analytical solution $\rho_{kk}(t) = \sum_{i,j} c_{ij} \exp(\Lambda_i(t-t_0)) \rho_{jj}(t_0)$, where the smallest, in absolute value, nonzero eigenvalue Λ of the rate matrix Γ gives the time scale of the relaxation of the system towards equilibrium [5].

V. DYNAMICAL REGIMES AND VALIDITY OF THE APPROXIMATION SCHEMES: PHASE DIAGRAM

While the dynamics of a TLS can occur in the coherent or incoherent tunneling regime, for the DDS there's a

richer variety of dynamical regimes, due to the different energy scales involved in the problem.

Looking at the free DDS dynamics depicted in Fig. 3, we recognize three characteristic frequencies: $\Omega_2 \ll \Omega_1 \ll \Omega_0$. As discussed in Sec. II C, this is reflected by the presence of a slow tunneling dynamics, occurring at the time scale Ω_2^{-1} , a fast tunneling dynamics with frequency Ω_1 and the intra-well dynamics, which occurs on the shortest time scale Ω_0^{-1} . In the dissipative case the different oscillatory behaviors undergo damping/temperature dependent frequency shifts and are progressively suppressed at different dissipation regimes.

At intermediate damping and temperature the dynamical regimes are controlled by the behavior of the effective TLSs introduced in Sec. IV, as the natural description for the system passes from the energy representation to the localized one given by the DVR. It is thus suggestive to use the machinery existing for the spin-boson problem to give an indication of the boundaries between different dynamical regimes in the parameter space.

As discussed in Sec. IV, each effective TLS, denoted by $\{|Q_i\rangle, |Q_j\rangle\}$, has its tunneling element Δ_{ij} , bias ϵ_{ij} and characteristic distance $q_{ij} = Q_i - Q_j$. It follows that at fixed γ , the effective coupling K_{ij} to which a TLS is subject can be more or less strong, depending on its parameters. The effective damping strength, or Kondo parameter, for the TLS $\{|Q_i\rangle, |Q_j\rangle\}$ is defined by

$$K_{ij} = M\gamma q_{ij}^2 / (2\pi\hbar). \quad (36)$$

For a real symmetric TLS at $T = 0$, the value $K = 1/2$ corresponds to the transition from the coherent to the incoherent behavior, while at $K = 1$ the *localization* occurs, consisting in the complete inhibition of the tunneling, with the consequence that the particle doesn't leave the well where it was prepared. The coherent-to-incoherent transition temperature T^* as a function of the effective damping for the symmetric TLS is given by [14]

$$T^*(K) = \left(\frac{(2\pi)^K}{\pi K} \right)^{1/(1-K)} \frac{\hbar\Delta_r}{k_B}, \quad (37)$$

where $\Delta_r = \Delta(\Delta/\omega_c)^{K/(1-K)}$ ($K < 1$) is the renormalized tunneling element.

We exploit the decoupling of the DDS into effective TLSs, in conjunction with numerical tests, to identify the following dynamical regimes in the (γ, T) -space for the DDS: (a) - completely coherent regime, with coherent tunneling at both the slow (Ω_2^{-1}) and the fast (Ω_1^{-1}) tunneling time scales and coherent intra-well oscillations (Ω_0^{-1}); (b) - coherence at the fast tunneling time scale Ω_1^{-1} , with oscillations of the left/right well populations around a slow incoherent relaxation behavior and coherent intra-well dynamics; (c) - crossover regime, where the coherence is only at the level of intra-well motion (on the time scale Ω_0^{-1}); (d) incoherent regime, where the four populations relax incoherently to their equilibrium values.

The regions in the parameter space corresponding to

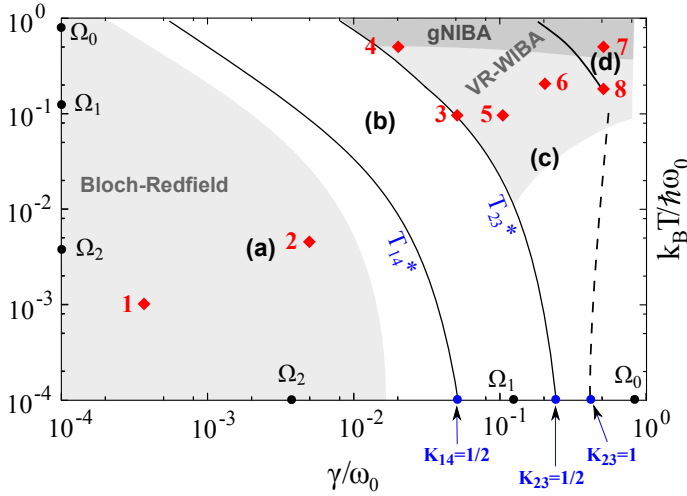


FIG. 8. (color online) Phase-space diagram in the dimensionless coupling-temperature space. The dynamical regions, separated by solid lines, are: (a) complete coherence, (b) coherent regime, (c) crossover regime and (d) incoherent regime. The dashed line is an extrapolation to finite temperatures of the localization regime predicted for the effective symmetric TLS $\{|Q_2\rangle, |Q_3\rangle\}$ at $T = 0$. The shaded areas indicate the validity domains of the approximation schemes used. The WR-WIBA reduces to the gNIBA at high temperatures, so the domain of the first scheme includes that of the latter. The characteristic frequencies Ω_i of the DDS, reported in both axes in units of ω_0 , serve as reference to establish the effective dissipation regimes. The diamonds refer to the parameters chosen to obtain the results presented in Sec. VI.

the above mentioned dynamical regimes and the validity areas of the approximation schemes used to treat the DDS are depicted in the phase diagram of Fig. 8.

The completely coherent regime (Region (a) on the phase diagram) is established by considering T_{14}^* , the coherent-to-incoherent transition temperature as a function of the effective coupling for the effective TLS $\{|Q_1\rangle, |Q_4\rangle\}$ (cf. Eq. (37)). The boundary between regions (a) and (b), given by T_{14}^* , determines the suppression of the slow oscillatory behavior of $P_L = \rho_{11} + \rho_{22}$, while both the intermediate tunneling oscillations and the fast intra-well dynamics survive.

In the part of Region (a) where the perturbative in the coupling treatment is appropriate, the Bloch-Redfield master equation describes correctly the dynamics of the DDS. The master equation has, for the coherences in the energy representation, the solution (see Appendix C)

$$\rho_{nm}^E(t) = e^{-i\omega_{nm}t} e^{-\mathcal{L}_{nm, nm}t} \rho_{nm}^E(t_0). \quad (38)$$

To determine the domain of validity of the Bloch-Redfield approach we compare the dephasing coefficient $\mathcal{L}_{12,12}$ with the frequency $\omega_{21} \equiv \Omega_2 = \omega_2 - \omega_1$ imposing $\mathcal{L}_{12,12} \leq \omega_{21}$. The result is the shaded area on the left part of the phase diagram. However, the extension of this validity domain may be overestimated, having

neglected the frequency shifts in the evaluation of the Bloch-Redfield tensor (see. Eq. C5). The weak coupling approximation fails near the boundary between (a) and (b) where the long time oscillations of P_L turn into incoherent relaxation.

Region (b) of the diagram, characterized by stronger damping and/or higher temperature, is outside the validity domain of the Bloch-Redfield approach. Nevertheless we can use the weak coupling estimates for the asymptotic values of the populations on the basis of the following argument. Whenever the relaxation to the equilibrium occurs, the asymptotic values of the left- and right-well populations are $P_L(\infty) = P_R(\infty) = 1/2$, due to the symmetry of the system. This means that we can obtain the single populations $\rho_{ii}(\infty)$, focusing on the intra-well biased TLSs $\{|Q_1\rangle, |Q_2\rangle\}$ and $\{|Q_3\rangle, |Q_4\rangle\}$. They are characterized by effective tunneling elements $|\Delta_{12}| \simeq 0.35\omega_0$ and effective biases $|\epsilon_{12}| \simeq 0.40\omega_0$. For these intra-well TLSs the effective damping $K_{12/34}$ is still weak and we can use the expressions given by the WCA [14] for the asymptotic populations of the intra-well TLSs states

$$\rho_{33/44}(\infty) = \frac{1}{4} \mp \frac{\epsilon}{4\Delta_b} \tanh\left(\frac{\hbar\Delta_b}{2k_B T}\right), \quad (39)$$

where $\Delta_b = \sqrt{\Delta_{12}^2 + \epsilon_{12}^2}$. By the symmetry of the problem we have $\rho_{22/11}(\infty) = \rho_{33/44}(\infty)$.

The boundary between the Regions (b) and (c) indicates the passage to the crossover regime in which the tunneling is incoherent. The right boundary to the area (b) is obtained considering the coherent-to-incoherent transition temperature T_{23}^* as a function of K_{23} for the symmetric TLS $\{|Q_2\rangle, |Q_3\rangle\}$.

The boundary between the coherent and the crossover regimes delimits also the validity of the approximation lying at the basis of the factorization of the DDS amplitudes into uncorrelated amplitudes relative to TLS paths. Indeed in the crossover regime, where the tunneling is incoherent, the contribution of the clusters in the sum over the paths is negligible so that the limitation made on the contributing paths holds.

Since the two intra-well TLSs have an effective bias, they can be treated according to the NIBA only in the high temperature/strong coupling regime (on the frequency scale Ω_0 of the intra-well motion) [14].

Treating the intra-well dynamics within the NIBA amounts to use the gNIBA scheme for the complete DDS and we can conclude that the gNIBA reproduces correctly the dynamics inside the darker shaded area in the uppermost part of the diagram.

The WIBA scheme applied to the intra-well TLSs extends the path integral approach for the DDS to low temperatures in a quite large damping range. The WIBA correctly predicts both the transient behavior and the asymptotic populations for the TLS whenever the intrablip correlation can be neglected (high temperature at any coupling) or treated to the first order (from low to high temperature at weak coupling) [32]. Thus the va-

lidity area of the VR-WIBA includes that of the gNIBA and covers the upper-right shaded region in the phase diagram.

The dissipation regime inaccessible to the WIBA for a biased TLS, and consequently to the VR-WIBA for the DDS, is the low temperature/intermediate-to-strong coupling, where the inter-blip correlations are non suppressed by the bath and the coupling is not sufficiently weak to justify their treatment to the first order in γ . This corresponds to the lower-right part of the diagram where the dashed line at strong damping indicates an extrapolation to finite temperatures of the localization regime occurring at $T = 0$ for the symmetric effective TLS $\{Q_2, Q_3\}$. The extrapolation is made observing that, in this region of the parameter space, the effective tunneling elements of the inter-well effective TLSs vanish [14], so that the DDS is not expected to undergo the tunneling dynamics, irrespective of the initial condition.

VI. RESULTS FOR THE DDS DYNAMICS

A. Parameters and units

We scale all the parameters with ω_0 , the natural oscillation frequency around the minima of the potential described in Eq. (2). We use the Ohmic bath spectral density function with exponential cutoff $J(\omega) = M\gamma\omega \exp(-\omega/\omega_C)$. The cutoff frequency is set to $\omega_C = 50\omega_0$. The potential is the same as in Fig. 2, with parameters $\epsilon = 0$ and $\Delta U = 1.4\hbar\omega_0$. In what follows $t_0 = 0$ and the initial condition is $\rho(0) = |Q_1\rangle\langle Q_1|$.

B. Dissipative DDS dynamics

In this section we show the time evolution of the populations in the DVR basis $|Q_1\rangle, \dots, |Q_4\rangle$, at the parameter space points indicated in the phase diagram (Fig. 8).

In the Region (a) of the phase diagram (completely coherent dynamical regime) we give the dynamics at two phase space points. The first one (Fig. 9), at very low T and γ , is well within the applicability domain of the Bloch-Redfield master equation. The dynamics of the left/right well populations, $P_{L/R}$, of the DDS shows a slow damped oscillatory behavior of frequency Ω_2 with superposed small oscillations of frequency Ω_1 featured also in the free dynamics (see Fig 3). The short time behavior of the single populations is shown in the lower panels and resembles the free case, with fast oscillations of frequency Ω_0 and an oscillatory envelope of frequency Ω_1 . This is because, at short times, the effect of the environment is not visible in this dissipation regime. We remark that in this dissipation regime the fast intra-well oscillations are a result of the initial condition (cf. Sec. IID).

The second dynamics is shown in Fig. 10 and corresponds to point 2 in the diagram. It is in the same dy-

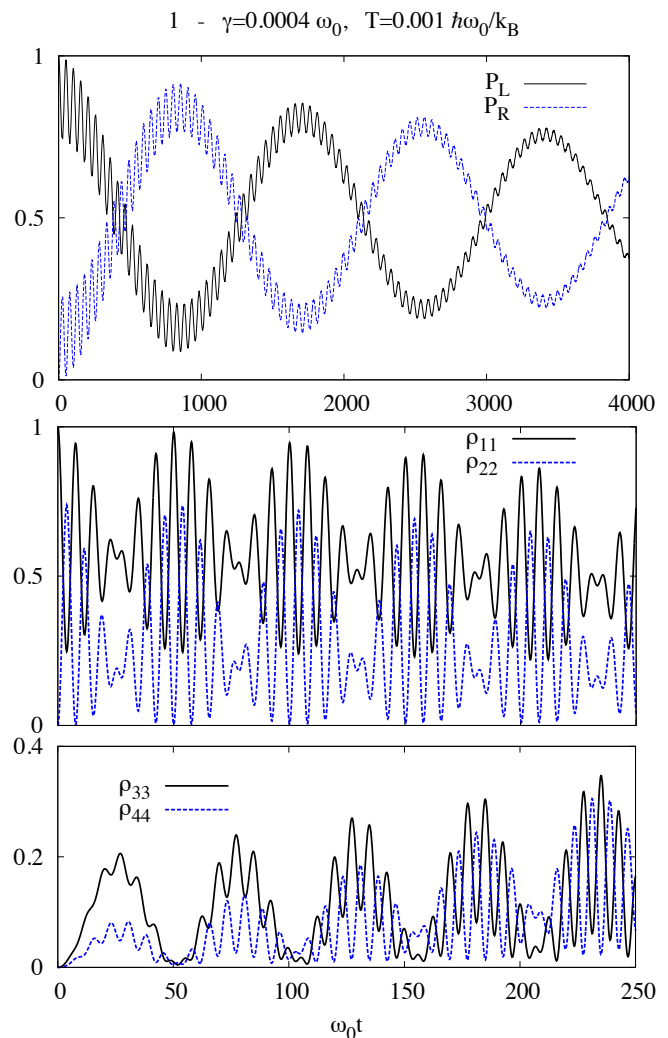


FIG. 9. (Color online) Completely coherent dynamics of the DDS at very weak damping and low temperature (point 1 in the phase diagram). Results obtained within the Bloch-Redfield master equation. *Uppermost panel* - Time evolution of the left/right well populations of the DDS. The long time behavior of $P_{L/R} = \rho_{11/33} + \rho_{22/44}$ is characterized by weakly damped oscillations of frequency Ω_2 and fast oscillations (of frequency Ω_1) around the long time envelope. Both these features are related to the tunneling dynamics. *Lowest panels* - Time evolution of the four populations in the DVR basis. The short time behavior of the DDS in this dissipation regime is very similar to the free case (see Fig 3).

namical regime as the first. The populations show the same qualitative feature as in the free case even if the damping of the fast tunneling oscillations is now visible.

The third point in the diagram is in the crossover regime at weak coupling and intermediate temperature (with respect to Ω_0). Here the coherence is only in the intra-well motion. In this dissipation regime the WCA completely fails as $\gamma \sim \Omega_1$, so the time evolution of the populations is calculated within the path integral ap-

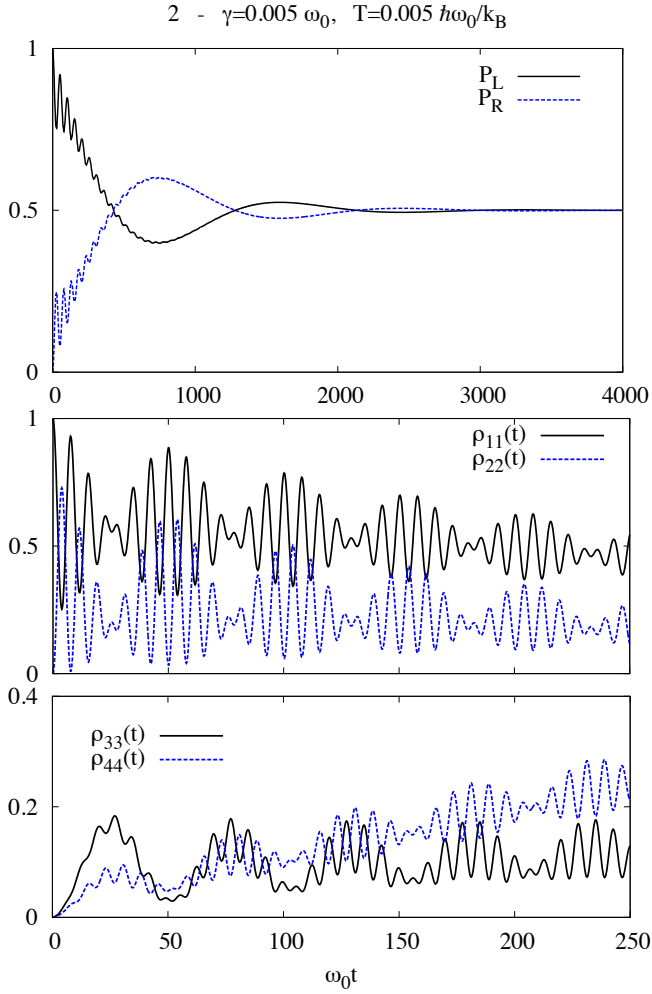


FIG. 10. (Color online) *Uppermost panel* - Time evolution of the left/right well populations of the DDS ($P_{L/R} = \rho_{11/33} + \rho_{22/44}$) for γ and T at point 2 in the phase diagram. The long time oscillations are more damped with respect to the case in the uppermost panel of Fig. 9. *Lowest panels* - Short time dynamics (with respect to Ω_2^{-1}) of the individual DDS populations. As in Fig. 9, the time evolutions display qualitatively the same features found in the free case (lower panel of Fig. 3) but the damping is now visible at this short time scale.

proach in the gNIBA and in the novel VR-WIBA scheme.

The results are given in Fig. 11 and show that the gNIBA fails as expected from the discussion in Sec. V. Indeed the point 3 in the phase diagram is outside the regime of validity of the gNIBA because the temperature is not sufficiently high to justify NIBA in the biased intra-well TLS.

The next time evolution is provided at point 4 in the diagram of Fig. 8, i.e. at weak damping and high temperature with respect to the intra-well frequency. Contrary to the previous case, here both the VR-WIBA and the gNIBA are expected to give the correct prediction. The results for the two schemes at this point of the parameter

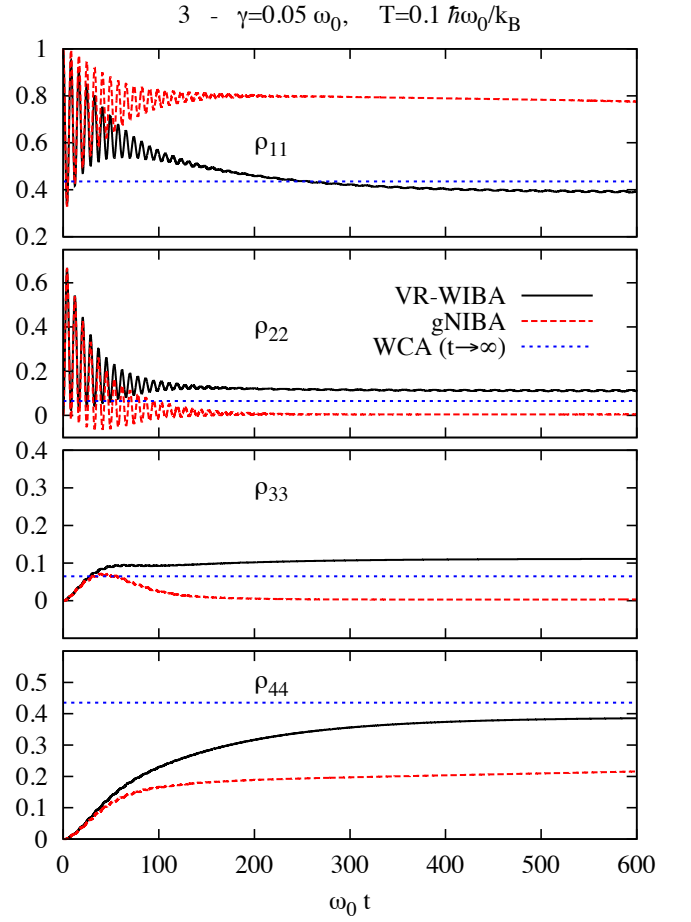


FIG. 11. (color online) Weak damping and low to intermediate temperature with respect to the intra-well frequency (point 3 in the phase diagram). Comparison between the VR-WIBA and the gNIBA results for the time evolution of the populations in the crossover dynamical regime (Region (c) in Fig. 8). As expected, the gNIBA gives incorrect predictions of both the transient and the stationary, while the VR-WIBA is expected to give the correct results. The configuration at equilibrium, as given by the WCA (Eq. (39)), is shown for comparison.

space coincide, as shown in Fig. 12.

The point 5 in the phase diagram is inside the crossover region at intermediate damping and temperature with respect to Ω_0 . The gNIBA and VR-WIBA dynamics are shown in Fig. 13. Similarly to the case 3, the gNIBA fails and the VR-WIBA is expected to give the correct predictions. Interestingly, even if the damping is larger than that at point 3 in the phase diagram, the gNIBA prediction in this case is even worse than in Fig. 11, as it predicts localization. This is because the beyond-NIBA correction in the intra-well kernels on the GME is proportional (at appropriate damping) to the damping itself (see Appendix B).

The sixth point in the diagram is in the strong coupling and intermediate to high temperature regime with

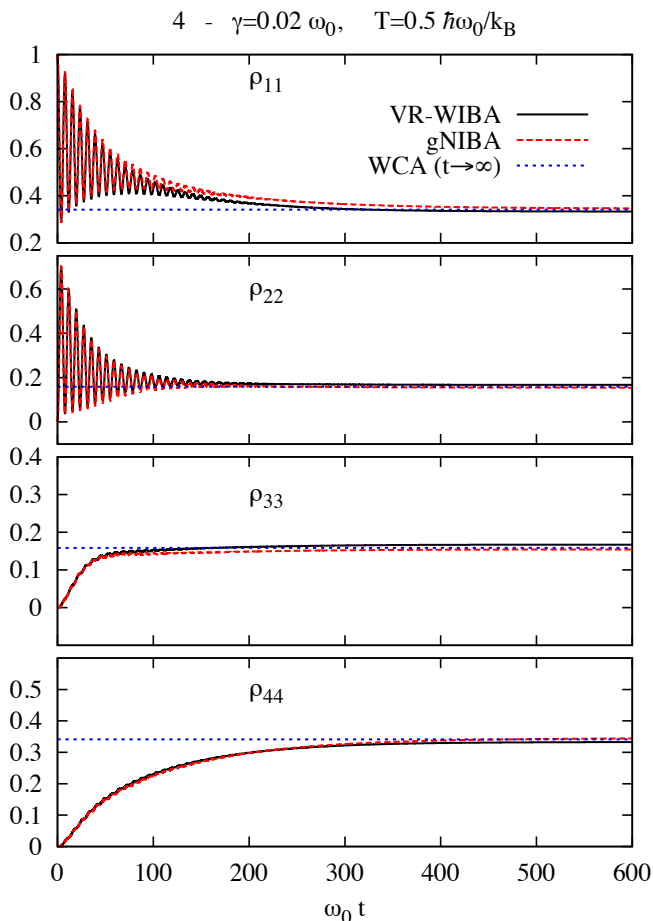


FIG. 12. (Color online) Weak damping and high temperature with respect to the intra-well frequency (point 4 in the phase diagram). Comparison between the VR-WIBA and the gNIBA results for the time evolution of the populations in the crossover dynamical regime (Region (c)). The results in the two scheme coincide and reproduce the correct stationary configuration, provided by the WCA (Eq. (39)). This example shows that the gNIBA scheme is reliable also at weak damping, provided that the temperature is high enough, according to the domain of validity established in Sec. V.

respect to the intra-well TLS parameters. The dynamical regime is the crossover (Region (c)) with strongly damped intra-well oscillations and slow incoherent tunneling relaxation. Again, the gNIBA results differ from those of the VR-WIBA, which confirms that also in this coupling regime the gNIBA is valid only at high temperatures.

The last two points (7 and 8 in the diagram of Fig. 8) are in the incoherent regime (Region (d)). The gNIBA describes well the incoherent relaxation at strong damping and high temperature, as shown in Fig. 15. In the strong coupling regime at intermediate temperatures (point 8) the gNIBA fails. The VR-WIBA is expected to give better results even if the treatment of the inter-blip interactions to the first order is questionable at this level

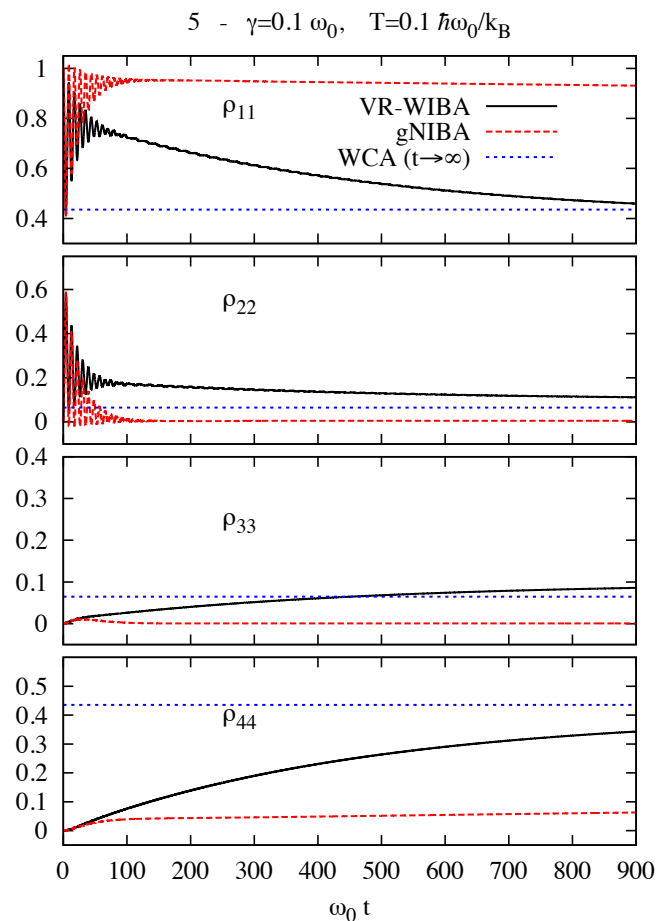


FIG. 13. (Color online) Intermediate damping and temperature with respect to the intra-well frequency (point 5 in the phase diagram). Comparison between the VR-WIBA and the gNIBA results for the time evolution of the populations in the crossover dynamical regime (Region (c)). As in Fig. 11 the gNIBA fails and the VR-WIBA is expected to be valid. The blue dashed lines are WCA prediction for the equilibrium values of the populations.

of coupling with the environment. The comparison of the WIBA with numerically exact approaches (QUAPI [36]) for the asymmetric TLS, in the strong dissipation regime, proves that the WIBA attains a good performance also outside the weak coupling limit at finite temperature [32].

VII. CONCLUSIONS

In this work we give a comprehensive account of the dissipative dynamics of the double-doublet system in an Ohmic environment with a high frequency cutoff, using a novel approximation scheme based on a real-time path integral approach, the VR-WIBA.

By taking into account the nonlocal inter-blip correlations at the level of the intra-well dynamics, this scheme contains and extends the domain of validity of the gener-

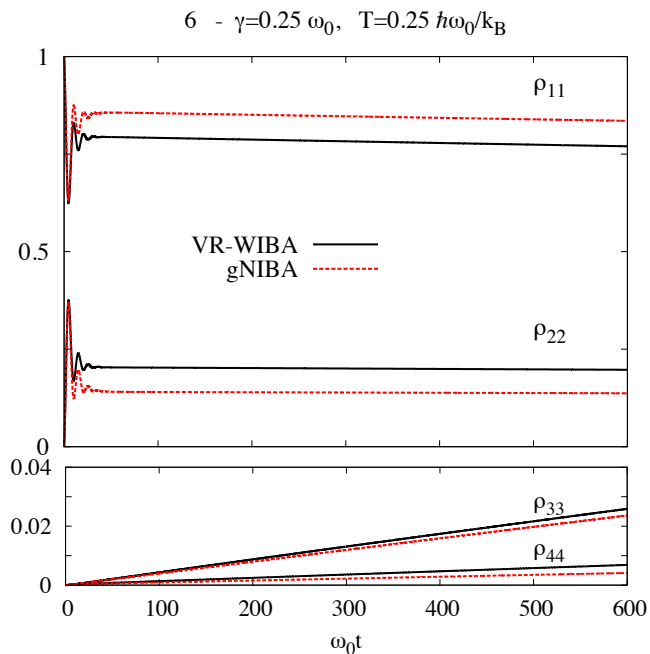


FIG. 14. (Color online) Strong damping and intermediate to high temperature with respect to the intra-well frequency (point 6 in the phase diagram). Comparison between the VR-WIBA and the gNIBA results for the time evolution of the populations in the strong coupling part of the crossover dynamical regime (Region (c)). The gNIBA and VR-WIBA results disagree as the coordinates of point 6 in the diagram are outside the gNIBA validity domain.

alized NIBA and succeeds in describing the crossover dynamical regime occurring at intermediate temperatures for a broad range of damping. The crossover regime is characterized by coherence at the level of intra-well motion and incoherent tunneling dynamics and is, to a large extent, inaccessible to previous approximation schemes.

At weak damping and low temperatures we use a Born-Markov approximated master equation technique to account for the coherent oscillatory behavior of the intra-well and tunneling dynamics. This approach is also used to check the VR-WIBA predictions for the stationary configuration where the damping is large respect to the tunneling frequency but still weak with respect to the intra-well characteristic frequency.

The combined use of the master equation and path integral techniques, within our novel scheme, accounts for the dissipative dynamics of the DDS in a large region of the parameter space where the four-state truncation of the Hilbert space is justified. To show this, we establish a phase diagram which describes the dynamics corresponding to the various dissipation regimes and the domains of validity of the techniques used in this work. We provide several examples of DDS dynamics in each of the accessible dynamical regimes in the phase diagram, ranging from the weak coupling/low temperature to the strong coupling/high temperature regime.

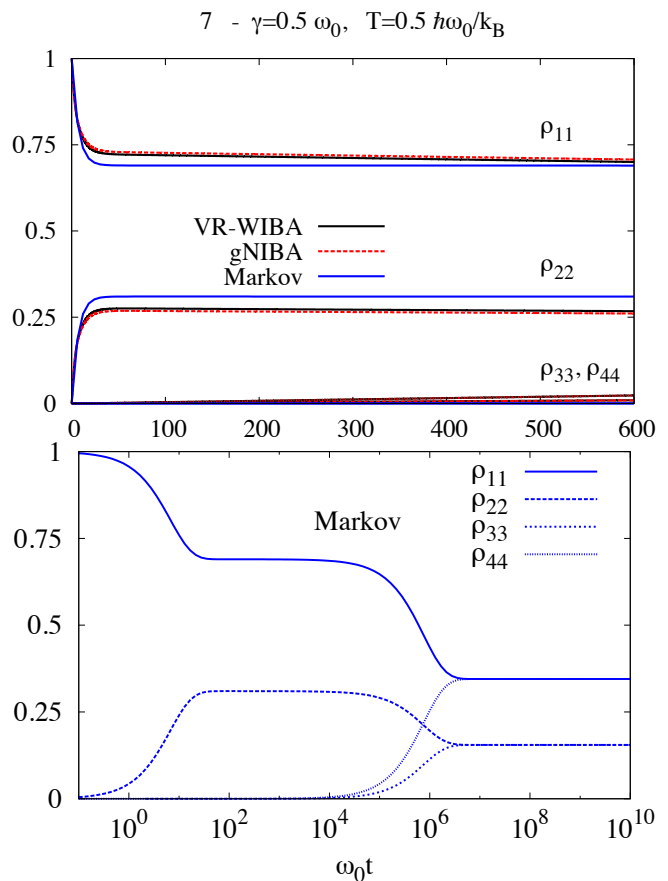


FIG. 15. (Color online) Incoherent dynamics at strong damping and high temperature (point 7 in the phase diagram). This dissipation regime is in the overlap of the validity domains of VR-WIBA and gNIBA. As expected, the results in the two schemes agree. *Upper panel* - Short time dynamics within the two approximation schemes; comparison with the Markov approximated gNIBA master equation (Eq. 35)). *Lower panel* - Long time dynamics (time in log scale) calculated by the gNIBA Markovian master equation.

Two final remarks are in order. Even if the calculations presented in this work are performed for an unbiased double well potential, the applicability of the VR-WIBA is not limited to the symmetric case. Indeed a static bias can be taken into account as long as the dynamical time scales of the intra- and inter-well dynamics remain well separated. In terms of energy levels, this means that the inter-doublet energy separation should be much larger than the intra-doublet separation. This condition is not very restrictive as it is fulfilled for any bias for which the two energy doublets are below the top of the potential barrier.

Finally, the generalization of the VR-WIBA to broadband sub-Ohmic or super-Ohmic environments is possible, although care must be taken in establishing, from time to time, the validity of the approximations discussed throughout this work.

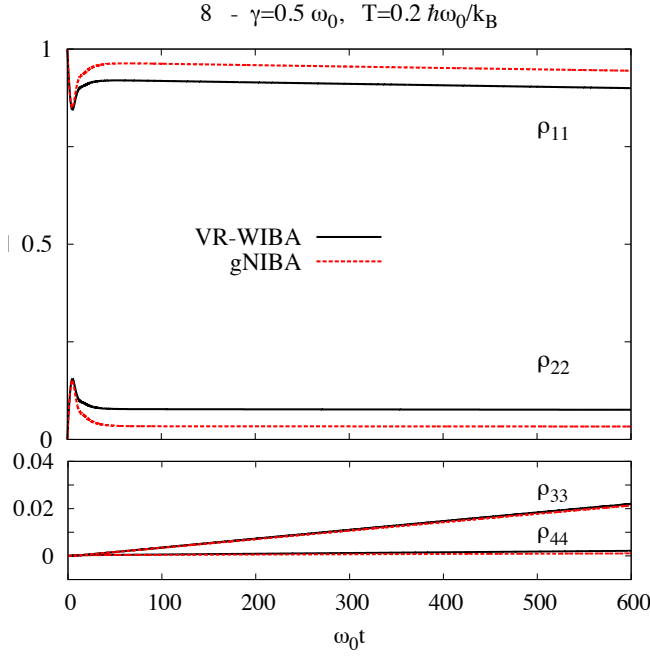


FIG. 16. (Color online) Strong damping and intermediate temperature (point 8 in the phase diagram). This regime is outside the reach of the gNIBA scheme, as shown in Fig. 8. Nevertheless the gNIBA predictions are in qualitative agreement with those of the VR-WIBA.

ACKNOWLEDGMENTS

We acknowledge financial support from the Collaborative Research Project SFB 631. This work was partially supported by MIUR through Grant. No. PON02_00355_3391233, Tecnologie per l'ENERGIA e l'Efficienza enERGETICa - ENERGETIC.

Appendix A: Propagator in Laplace space

First we give the expressions for the blip times τ and the sojourn times σ

$$\begin{aligned}\tau_j &= t_{2j} - t_{2j-1} \\ \sigma_j &= t_{2j+1} - t_{2j}.\end{aligned}$$

The approximation on the paths made in Sec. IV A implies that, if $\rho(t_0) = |Q_j\rangle\langle Q_j|$, then each path contributing to the population $\rho_{kk}(t)$ has an even number $2n$ of transitions. Consider the series of integrals

$$\int_{t_0}^t dt_{2n} \int_{t_0}^{t_{2n}} dt_{2n-1} \dots \int_{t_0}^{t_3} dt_2 \int_{t_0}^{t_2} dt_1. \quad (\text{A1})$$

Using repeatedly the integral interchange rule

$$\int_{t_0}^{t_{j+1}} dt_j \int_{t_0}^{t_j} dt_{j-1} = \int_{t_0}^{t_{j+1}} dt_{j-1} \int_{t_{j-1}}^{t_{j+1}} dt_j, \quad (\text{A2})$$

we can put Eq. (A1) in the form

$$\begin{aligned}& \int_{t_0}^t dt_1 \int_{t_1}^t dt_2 \int_{t_2}^t dt_3 \dots \int_{t_{2n-2}}^t dt_{2n-1} \int_{t_{2n-1}}^t dt_{2n} \\ &= \int_0^{\bar{t}} d\sigma_0 \int_0^{\bar{t}-\sigma_0} d\tau_1 \int_0^{\bar{t}-\tau_1-\sigma_0} d\sigma_1 \dots \\ & \quad \times \int_0^{\bar{t}-\dots-\tau_{n-1}} d\sigma_{n-1} \int_0^{\bar{t}-\dots-\sigma_{n-1}} d\tau_n.\end{aligned}$$

Notice that there is no integration over the last sojourn time, since it is fixed by the length of the interval $\bar{t} = t - t_0$.

In passing to the Laplace space we note that $\bar{t} = \sigma_n + \tau_n + \dots + \tau_1 + \sigma_0$. Using repeatedly the rule $\int_0^\infty dt \int_0^t dt' = \int_0^\infty dt' \int_{t'}^\infty dt$, we obtain

$$\begin{aligned}\mathcal{L}_{\bar{t}} & \int_0^{\bar{t}} d\sigma_0 \dots \int_0^{\bar{t}-\dots-\sigma_{n-1}} d\tau_n \\ &= \int_0^\infty d\bar{t} e^{-\lambda \bar{t}} \int_0^{\bar{t}} d\sigma_0 \dots \int_0^{\bar{t}-\dots-\sigma_{n-1}} d\tau_n \\ &= \int_0^\infty d\sigma_n e^{-\lambda \sigma_n} \int_0^\infty d\tau_n e^{-\lambda \tau_n} \dots \int_0^\infty d\sigma_0 e^{-\lambda \sigma_0}.\end{aligned} \quad (\text{A3})$$

Suppose that a path of the DDS with $2n$ transitions starts in the diagonal state (q_0, q_0) and ends in the diagonal state (q, q) . Suppose moreover that the path changes sublattice M times. Specifically it passes from (q_0, q_0) to (q_1, q_1) making $2k_1$ transitions in the first sublattice, then passes from (q_1, q_1) to (q_2, q_2) making $2k_2$ transitions in the second sublattice and so on, with $\sum_{j=1}^M k_j = n$. Notice that the starting and arrival sites of the sub-paths need not to be different. Due to the approximations made in Sec. IV, the amplitude A for this path factorizes as

$$A(\tau_1, \sigma_1, \dots, \sigma_{n-1}, \tau_n) = \prod_{j=1}^M A_j(\tau_1^j, \sigma_1^j, \dots, \sigma_{k_j-1}^j, \tau_{k_j}^j).$$

Here τ_i^j (σ_i^j) is the i -th blip (sojourn) in the j -th sublattice (see Figs. 7 and 8). Therefore the Laplace transform of the multiple integral of the amplitude A is

$$\mathcal{L}_{\bar{t}} \int_0^{\bar{t}} d\sigma_0 \dots \int_0^{\bar{t}-\dots-\sigma_{n-1}} d\tau_n A(\tau_1, \dots, \tau_n) = \frac{1}{\lambda} \prod_{j=1}^M \frac{\hat{f}_j(\lambda)}{\lambda}, \quad (\text{A4})$$

where

$$\begin{aligned}\frac{\hat{f}_j(\lambda)}{\lambda} &= \int_0^\infty d\tau_{k_j}^j e^{-\lambda \tau_{k_j}^j} \dots \int_0^\infty d\sigma_0^j e^{-\lambda \sigma_0^j} A_j(\tau_1^j, \dots, \tau_{k_j}^j) \\ &= \mathcal{L}_T \int_0^T d\tau_1^j \dots \int_0^{T-\dots-\sigma_{k_j-1}^j} d\tau_{k_j}^j A_j(\tau_1^j, \dots, \tau_{k_j}^j),\end{aligned}$$

with σ_0^j playing the role of σ_n in Eq. (A3): the integral over the sojourn times results in the $1/\lambda$ factors because none of the amplitudes depend on the initial or final sojourn time.

The full propagator from (q_0, q_0) to (q, q) is the sum over the paths

$$G(q, q, t; q_0, q_0, t_0) = \delta_{qq_0} + \sum_{n=1}^{\infty} \int_{t_0}^t \mathcal{D}_{2n}\{t_j\} A(t_0, \dots, t). \quad (\text{A5})$$

Exploiting the factorization of the amplitudes in this sum and extending the reasoning made above for a single amplitude, the Laplace transform of the propagator is

$$G(q, q; q_0, q_0; \lambda) = \frac{\delta_{qq_0}}{\lambda} + \frac{1}{\lambda} \sum_{M=1}^{\infty} \sum_{\{q_j\}=Q_1}^{Q_4} \prod_{j=1}^M \frac{\hat{K}_{q_{j-1}q_j}(\lambda)}{\lambda} \quad (\text{A6})$$

where, if $q_j \neq q_{j-1}$, the function $\hat{K}_{q_{j-1}q_j}(\lambda)$ is the Laplace transform of

$$K_{j,j-1}(t-t') = \sum_{k_j=1}^{\infty} \int_{t'}^t dt_{2k_j-1} \dots \int_{t'}^t dt_{2k_j} \\ \times \sum_{\text{paths}_{2k_j}} A_j^{q_{j-1}, q_j}(t, t_{2k_j-1}, \dots, t').$$

This, in turn, is the kernel that connects the populations of the states $|q_{j-1}\rangle$ and $|q_j\rangle$ in the integro-differential equation [14, 37]

$$\dot{\rho}_{q_j q_j}(t) = \sum_{l=q_{j-1}}^{q_j} \int_{t_0}^{t_{2k}} dt_1 K_{q_j, l}(t-t') \rho_{ll}(t')$$

for the populations of the TLS $\{|q_{j-1}\rangle, |q_j\rangle\}$ corresponding to the j -th sublattice $\{q_{j-1}, q_j\}$.

Appendix B: VR-WIBA kernels

The gNIBA kernels connecting the populations of the states $|q_k\rangle$ and $|q_j\rangle$ in Eq. (34) are the modified versions of the TLS NIBA kernels

$$K_{kj}^N(t) = 2\Delta_{kj}^2 e^{-q_{kj}^2 Q'(t)} \cos(\epsilon_{kj}t + q_{kj}^2 Q''(t)) \quad (\text{B1})$$

where

$$\Delta_{kj} = \frac{1}{\hbar} \langle q_k | \hat{H}_S | q_j \rangle \\ \epsilon_{kj} = \frac{1}{\hbar} \left(\langle q_k | \hat{H}_S | q_k \rangle - \langle q_j | \hat{H}_S | q_j \rangle \right) \\ q_{kj}^2 = (q_k - q_j)^2.$$

In the VR-WIBA scheme we use these expressions only if q_k and q_j belong to different wells.

If q_k and q_j belong to the same well, we use the modified TLS WIBA kernels (see Ref. [32]) $K_{kj}^W(t) =$

$K_{kj}^N(t) + K_{kj}^{BN}(t)$. The beyond-NIBA correction is

$$K_{kj}^{BN}(t) = 8\Delta_{kj}^4 \int_0^t d\tau \int_0^{t-\tau} d\tau' e^{-q_{kj}^2 Q'(\tau) - q_{kj}^2 Q'(\tau')} \\ \times \sin(\epsilon_{kj}\tau') \cos(q_{kj}^2 Q''(\tau')) p_{kj}(t-\tau-\tau') \\ \times [q_{kj}^2 X(t, \tau') \cos(\epsilon_{kj}\tau + q_{kj}^2 Q''(\tau)) \\ - q_{kj}^2 \Lambda(t, \tau', \tau) \sin(\epsilon_{kj}\tau + q_{kj}^2 Q''(\tau))], \quad (\text{B2})$$

where

$$\Lambda(t, \tau', \tau) = Q'(t) + Q'(t-\tau'-\tau) - Q'(t-\tau) - Q'(t-\tau')$$

and

$$X(t, \tau') = Q''(t) - Q''(t-\tau').$$

In the calculations the function $Q'(t)$ and $Q''(t)$ are taken in the form of Eq. (27).

The functions p_{kj} obey the equations

$$\dot{p}_{kj}(t) = \int_0^t dt' K_{kj}^{N,(+)}(t-t') p_{kj}(t')$$

with initial condition $p_{kj}(0) = 1$ and kernel

$$K_{kj}^{N,(+)}(\tau) = -4\Delta_{kj}^2 e^{-q_{kj}^2 Q'(\tau)} \cos(\epsilon_{kj}\tau) \cos(q_{kj}^2 Q''(\tau)).$$

Note that, by the symmetry of the problem, the four functions p_{12}, p_{21}, p_{34} and p_{43} are the same for the symmetric DDS.

Appendix C: Bloch-Redfield master equation

The energy representation of the DDS is given by the four energy eigenstates $|n\rangle$ satisfying the equations

$$\hat{H}_S |n\rangle = \hbar\omega_n |n\rangle \quad (n = 1, \dots, 4).$$

We define

$$\omega_{nm} = \omega_n - \omega_m \quad \text{and} \quad q_{nm} = \langle n | \hat{q} | m \rangle.$$

In the energy representation, to the first order in the coupling and under the assumption that the memory time of the bath is short compared to the characteristic times in the evolution of the density matrix (Markov approximation), the following master equation can be derived [24] from the microscopical model given in Sec. II

$$\dot{\rho}_{nm}^E(t) = -i\omega_{nm} \rho_{nm}^E(t) + \sum_{k,l} \mathcal{L}_{nm,kl} \rho_{kl}^E(t). \quad (\text{C1})$$

This is the *Bloch-Redfield master equation*. The Bloch-Redfield tensor is

$$\mathcal{L}_{nm,kl} = q_{nk} (Q_{lm} + P_{lm}) + q_{lm} (Q_{nk} - P_{nk}) \\ - \sum_j [\delta_{kn} q_{jm} (Q_{lj} + P_{lj}) + \delta_{lm} q_{nj} (Q_{jk} - P_{jk})] \quad (\text{C2})$$

where

$$Q_{nm} = q_{nm} \int_0^\infty d\tau \int_0^\infty d\omega \frac{J(\omega)}{\pi\hbar} \times \coth\left(\frac{\beta\hbar\omega}{2}\right) \cos(\omega\tau) e^{-i\omega_{nm}\tau} \quad (\text{C3})$$

and

$$P_{nm} = q_{nm}\omega_{nm} \int_0^\infty d\tau \int_0^\infty d\omega \frac{J(\omega)}{\omega\pi\hbar} \cos(\omega\tau) e^{-i\omega_{nm}\tau}. \quad (\text{C4})$$

To perform the integral over τ we use

$$\int_0^\infty d\tau e^{i\tilde{\omega}\tau} = \pi\delta(\tilde{\omega}) + i\mathcal{P}\frac{1}{\tilde{\omega}}. \quad (\text{C5})$$

Neglecting the principal value, which gives a frequency shift, we have

$$Q_{nm} = q_{nm} \frac{J(|\omega_{nm}|)}{2\hbar} \coth\left(\frac{\beta\hbar|\omega_{nm}|}{2}\right) \quad (\text{C6})$$

and

$$P_{nm} = \frac{q_{nm}\omega_{nm}}{2\hbar} \frac{J(|\omega_{nm}|)}{|\omega_{nm}|}. \quad (\text{C7})$$

We notice that for $\omega_{nm} > 0$

$$Q_{nm} - P_{nm} = Q_{mn} + P_{mn} = q_{nm} \frac{J(|\omega_{nm}|)}{\hbar} n_\beta(\omega_{nm})$$

while, for $\omega_{nm} < 0$,

$$Q_{nm} - P_{nm} = Q_{mn} + P_{mn} = q_{nm} \frac{J(|\omega_{nm}|)}{\hbar} (n_\beta(|\omega_{nm}|) + 1).$$

Here $n_\beta(\omega_{nm})$ is the expectation value of the number of bath excitations of energy $\hbar\omega_{nm}$ at temperature $T = (k_B\beta)^{-1}$.

1. Analytic solution in the full secular approximation

Setting $\rho_{nm}^E(t) = e^{-i\omega_{nm}(t-t_0)}\sigma_{nm}(t)$, Eq. (C1) becomes

$$\dot{\sigma}_{nm}(t) = \sum_{kl} \mathcal{L}_{nm,kl} \Omega_{nm,kl}(t) \sigma_{kl}(t), \quad (\text{C8})$$

where $\Omega_{nm,kl}(t) = \exp[i(\omega_{nm} - \omega_{kl})(t - t_0)]$. We have $\sigma(t_0) = \rho(t_0)$.

The *full secular approximation* (FSA) consists in neglecting the terms in the master equation for which $\omega_{\mu\nu} - \omega_{\kappa\lambda} \neq 0$. Mathematically this condition reads

$$\Omega_{\mu\nu\kappa\lambda}(t) \rightarrow (\delta_{\kappa\mu}\delta_{\lambda\nu} + \delta_{\kappa\lambda}\delta_{\mu\nu})\Omega_{\mu\nu\kappa\lambda}(t).$$

In the FSA the equations for the diagonal elements decouple from those for the non-diagonal elements of σ .

Specifically, the dynamics of $\sigma(t)$ is given by a master equation for the diagonal elements and a set of independent equations for the *non-diagonal* elements. The master equation for the diagonal elements reads

$$\dot{\sigma}_{nn}(t) = \sum_k \mathcal{L}_{nn,kk} \sigma_{kk}(t), \quad (\text{C9})$$

where, for $n \neq k$,

$$\mathcal{L}_{nn,kk} = q_{nk}(Q_{kn} + P_{km}) + q_{kn}(Q_{nk} - P_{nk})$$

and $\mathcal{L}_{n,n} = -\sum_k \mathcal{L}_{k,n}$.

The solution of Eq. (C9) is

$$\sigma_{nn}(t) = \sum_{ij} S_{ni} e^{\lambda_i(t-t_0)} (S^{-1})_{ij} \sigma_{jj}(t_0),$$

where S is the transformation that diagonalizes the matrix $L_{nk} = \mathcal{L}_{nn,kk}$ and λ_i are the eigenvalues. From the definition of $\sigma(t)$ we have $\rho_{nn}^E(t) = \sigma_{nn}(t)$.

The uncoupled equations for the non-diagonal elements of $\sigma(t)$ are

$$\dot{\sigma}_{nm}(t) = -\mathcal{L}_{nm,nm} \sigma_{nm}(t) \quad (\text{C10})$$

with

$$\begin{aligned} \mathcal{L}_{nm,nm} = & (q_{nn} - q_{mm}) [Q_{nn} - P_{nn} - (Q_{mm} + P_{mm})] \\ & + \sum_{j \neq m} q_{jm} (Q_{mj} + P_{mj}) + \sum_{j \neq n} q_{nj} (Q_{jn} - P_{jn}). \end{aligned}$$

In our specific problem, due to the symmetry of the potential, the diagonal matrix elements q_{ii} of the position operator in the energy representation vanish.

The solutions of Eq. (C10) are

$$\sigma_{nm}(t) = e^{-\mathcal{L}_{nm,nm}(t-t_0)} \sigma_{nm}(t_0),$$

so that the non-diagonal elements of the density matrix in the energy representation are

$$\rho_{nm}^E(t) = e^{-i\omega_{nm}(t-t_0)} e^{-\mathcal{L}_{nm,nm}(t-t_0)} \rho_{nm}^E(t_0).$$

Once the solution for $\rho(t)$ in the energy basis $\{|n\rangle\}$ is known, to pass to the DVR basis $\{|q_j\rangle\}$ it is sufficient to perform the transformation

$$\rho_{nm}^{DVR}(t) = \sum_{ij} T_{ni} \rho_{ij}^E(t) T_{jm}^\dagger,$$

where $T_{ij} = \langle i|q_j\rangle$.

-
- [1] I. Chiorescu, Y. Nakamura, C. J. P. M. Harmans, and J. E. Mooij, *Science* **299**, 1869 (2003).
- [2] F. Chiarello *et al.*, *New J. Phys.* **14** (2012).
- [3] S. Takahashi *et al.*, *Phys. Rev. Lett.* **102**, 087603 (2009).
- [4] M. Thorwart, M. Grifoni, and P. Hänggi, *Phys. Rev. Lett.* **85**, 860 (2000).
- [5] M. Thorwart, M. Grifoni, and P. Hänggi, *Ann. Phys.* **293**, 15 (2001).
- [6] P. Caldara *et al.*, *Int. Journ. of Quant. Inf.* **09**, 119 (2011).
- [7] B. Spagnolo *et al.*, *International Journal of Modern Physics B* **26**, 1241006 (2012).
- [8] L. Magazzù *et al.*, *Acta Phys. Pol. B* **44**, 1185 (2013).
- [9] M. H. Devoret and R. J. Schoelkopf, *Science* **339**, 1169 (2013).
- [10] J. You and F. Nori, *Nature* **474**, 589 (2011).
- [11] T. D. Ladd *et al.*, *Nature* **464**, 45 (2010).
- [12] J. Clarke and F. Wilhelm, *Nature* **453**, 1031 (2008).
- [13] M. Devoret and J. Martinis, *Quantum Inf. Process.* **3**, 163 (2004).
- [14] U. Weiss, *Quantum Dissipative Systems* (World Scientific, Singapore, 2012, 4th ed.).
- [15] E. Paladino, Y. M. Galperin, G. Falci, and B. L. Altshuler, *Rev. Mod. Phys.* **86**, 361 (2014).
- [16] A. J. Leggett *et al.*, *Rev. Mod. Phys.* **59**, 1 (1987); erratum, *ibid.* **67**, 725 (1995).
- [17] H. Dekker, *Physica A: Statistical Mechanics and its Applications* **175**, 485 (1991); **176**, 220 (1991); **179**, 81 (1991).
- [18] R. I. Cukier, M. Morillo, K. Chun, and N. O. Birge, *Phys. Rev. B* **51**, 13767 (1995).
- [19] M. Morillo, C. Denk, and R. Cukier, *Chem. Phys* **212**, 157 (1996).
- [20] R. Cukier, C. Denk, and M. Morillo, *Chem. Phys* **217**, 179 (1997).
- [21] R. P. Feynman and F. Vernon Jr, *Ann. Phys.* **24**, 118 (1963).
- [22] K. L. Hur, *Annals of Physics* **323**, 2208 (2008).
- [23] A. Caldeira and A. Leggett, *Phys. Rev. Lett.* **46**, 211 (1981).
- [24] K. Blum, *Density matrix theory and applications*, Vol. 64 (Springer, 2012).
- [25] N. Makri and D. Makarov, *J. Chem. Phys.* **102**, 4600 (1995).
- [26] R. Egger and C. H. Mak, *Phys. Rev. B* **50**, 15210 (1994).
- [27] J. T. Stockburger and H. Grabert, *Phys. Rev. Lett.* **88**, 170407 (2002).
- [28] W. Koch, F. Großmann, J. T. Stockburger, and J. Ankerhold, *Phys. Rev. Lett.* **100**, 230402 (2008).
- [29] P. P. Orth, A. Imambekov, and K. Le Hur, *Phys. Rev. B* **87**, 014305 (2013).
- [30] H. P. Breuer and F. Petruccione, *The theory of open quantum systems* (Oxford University Press, 2002).
- [31] R. Görlich, M. Sassetti, and U. Weiss, *Europhys. Lett.* **10**, 507 (1989).
- [32] F. Nesi, E. Paladino, M. Thorwart, and M. Grifoni, *Phys. Rev. B* **76**, 155323 (2007).
- [33] D. O. Harris, G. G. Engerholm, and W. D. Gwinn, *J. Chem. Phys.* **43**, 1515 (1965).
- [34] H. Grabert, P. Schramm, and G.-L. Ingold, *Phys. Rep.* **168**, 115 (1988).
- [35] F. Nesi, *Characterization of a qubit in presence of dissipation and external driving*, Phd thesis, Universität Regensburg (2007).
- [36] D. Makarov and N. Makri, *Phys. Rev. B* **52**, R2257 (1995).
- [37] M. Grifoni, M. Sassetti, and U. Weiss, *Phys. Rev. E* **53**, R2033 (1996).